Thermal Oxidation Profiling of Single-Walled Carbon Nanotubes

Brian J. Landi,[†,‡] Cory D. Cress,[†,‡] Chris M. Evans,[†] and Ryne P. Raffaelle*[,†,‡,§]

NanoPower Research Laboratories (NPRL), Department of Microsystems Engineering, and Department of Physics, Rochester Institute of Technology, Rochester, New York 14623

Received September 5, 2005. Revised Manuscript Received October 27, 2005

The use of thermal oxidation profiling (TOP) to monitor the properties of single-walled carbon nanotube (SWNT)-containing samples at incremental temperature intervals has been developed. Specifically, the thermal decomposition of raw and acid-refluxed SWNT samples is evaluated by a systematic series of oxidative thermal treatments with concomitant purity assessment to ascertain the SWNT mass retention. The TOP results, supported by Raman spectroscopy, indicate that the SWNT decomposition coincides with the onset of raw soot combustion. The temperature for this SWNT combustion onset is equivalent to pure metal-catalyst oxidation, particularly for the highly exothermic Co metal. Thus, there are no discernible regions of a raw soot thermogravimetric analysis (TGA) curve that can be ascribed to SWNT combustion independent of metal impurity influence. In contrast, the acid-refluxed SWNT sample shows that chemical oxidation of the metal can enable optimization of SWNT retention during thermal purification. The established understanding between time and temperature on thermal oxidation allows for purification efficiencies (the highest purity at the maximum retention) of 75% w/w to be achieved in laser-produced SWNTs, without modification to the diameter distribution.

Introduction

Single-walled carbon nanotubes (SWNTs) are being investigated for a variety of applications based on their unique electrical, optical, and mechanical properties.[1−4] While such properties are truly significant, the practical realization of reproducible performance in devices (e.g., field-effect transistors,[5] chemical and biosensors,[6] polymeric actuators,[7] Li^+ batteries and supercapacitors,[8] etc.) will require material standardization, especially in terms of electronic type and degree of purity. In addition, there is a pressing demand by researchers for quality verification and consistency of SWNT samples from commercial sources.[9] There have been various experimental methods reported in regard to the synthesis of SWNTs (i.e., arc-discharge, chemical vapor deposition, and pulsed laser vaporization).[1−3] Each technique produces SWNTs with differing diameter, chirality distributions, and various amounts of synthesis byproducts (amorphous carbon, metal catalysts, fullerenes, etc.). A variety of reports have assessed the quality of such materials through electron microscopy and spectroscopy,[10−12] but there is no single metric which accurately quantifies the types, amount, and morphology of SWNT-containing materials. In general, the most important criterion is the "purity", or quantity of SWNTs present in relation to other byproducts from the synthesis. Therefore, it is essential that a precise definition be established for both measurement and terminology as to what "purity" means in regard to SWNTs.[13] The development of a simple protocol to assess the purity of SWNTs has been sought after by many research groups.[13−21] SWNT purity assessment should rely on readily available techniques which measure quantities directly related to mass fraction, while analyzing a representative portion of the SWNT-containing sample. In addition, the accuracy of an approach must be verified in reference to a calibrated standard or known sample set. The implementation of well-understood characterization techniques which extract perti-

* Corresponding author e-mail: rprsps@rit.edu.
† NanoPower Research Laboratories.
‡ Department of Microsystems Engineering.
§ Department of Physics.

(1) Dai, H. *Surf. Sci.* **2002**, *500*, 218−241.
(2) Popov, V. N. *Mater. Sci. Eng., R* **2004**, *43*, 61−102.
(3) Raffaelle, R. P.; Landi, B. J.; Harris, J. D.; Bailey, S. G.; Hepp, A. F. *Mater. Sci. Eng., B* **2005**, *116*, 233−243.
(4) Ando, T. *Physica E* **2004**, *22*, 656−661.
(5) Avouris, P.; Appenzeller, J. *Ind. Phys.* **2004**, *10*, 18−21.
(6) Lin, Y.; Taylor, S.; Li, H.; Fernando, K. A. S.; Qu, L.; Wang, W.; Gu, L.; Zhou, B.; Sun, Y.-P. *J. Mater. Chem.* **2004**, *14*, 527−541.
(7) Landi, B. J.; Raffaelle, R. P.; Heben, M. J.; Alleman, J. L.; VanDerveer, W.; Gennett, T. *Nano Lett.* **2002**, *2*, 1329−1332.
(8) Frackowiak, E.; Beguin, F. *Carbon* **2002**, *40*, 1775−1787.
(9) Giles, J. *Nature* **2004**, *432*, 791.
(10) Arepalli, S.; Holmes, W. A.; Nikolaev, P.; Hadjiev, V. G.; Scott, C. D. *J. Nanosci. Nanotechnol.* **2004**, *4*, 762−773.
(11) Arepalli, S.; Nikolaev, P.; Gorelik, O.; Hadjiev, V. G.; Holmes, W.; Files, B.; Yowell, L. *Carbon* **2004**, *42*, 1783−1791.
(12) Itkis, M. E.; Perea, D. E.; Jung, R.; Niyogi, S.; Haddon, R. C. *J. Am. Chem. Soc.* **2005**, *127*, 3439−3448.
(13) Landi, B. J.; Ruf, H. J.; Evans, C. M.; Cress, C. D.; Raffaelle, R. P. *J. Phys. Chem. B* **2005**, *109*, 9952−9965.
(14) Dillon, A. C.; Gennett, T.; Parilla, P. A.; Alleman, J. L.; Jones, K. M.; Heben, M. J. *Mater. Res. Soc. Symp. Proc.* **2001**, *633*, A5.2.1−A5.2.6.
(15) Dillon, A. C.; Yudasaka, M.; Dresselhaus, M. S. *J. Nanosci. Nanotechnol.* **2004**, *4*, 691−703.
(16) Itkis, M. E.; Perea, D. E.; Niyogi, S.; Rickard, S. M.; Hamon, M. A.; Hu, H.; Zhao, B.; Haddon, R. C. *Nano Lett.* **2002**, *3*, 309.
(17) Jost, O.; Gorbunov, A. A.; Pompe, W.; Pichler, T.; Friedlein, R.; Knupfer, M.; Reibold, M.; Bauer, H.-D.; Dunsch, L.; Golden, M. S.; Fink, J. *Appl. Phys. Lett.* **1999**, *75*, 2217−2219.
(18) Kataura, H.; Kumazawa, Y.; Maniwa, Y.; Umezu, I.; Suzuki, S.; Ohtsuka, Y.; Achiba, Y. *Synth. Met.* **1999**, *103*, 2555−2558.
(19) Lobach, A. S.; Spitsina, N. G.; Terekhov, S. V.; Obraztsova, E. D. *Phys. Solid State* **2002**, *44*, 475−477.
(20) Ryabenko, A. G.; Dorofeeva, T. V.; Zvereva, G. I. *Carbon* **2004**, *42*, 1523.
(21) Terekhov, S. V.; Obraztsova, E. D.; Lobach, A. S.; Konov, V. I. *Appl. Phys. A* **2002**, *74*, 393−396.

10.1021/cm052002u CCC: $30.25
Published on Web 11/30/2005

nent information about the sample's quality will allow for the consistency demanded in SWNT-based devices.

The most popular techniques for SWNT characterization have been scanning electron microscopy (SEM), transmission electron microscopy (TEM), optical absorption spectroscopy, thermogravimetric analysis (TGA), and Raman spectroscopy.[3,10−12] The proper combination of these techniques, and possibly others, should provide an accurate account of the quality of SWNT samples. Unfortunately, many groups have used such techniques to report high purity levels, with several accounts >90% pure without reference to adequate material standards.[14,22−26] Electron microscopy (SEM and TEM) is commonly used to detect the presence of SWNTs, with some groups reporting purity levels (as a volume % at times) based on this qualitative, sample-limiting measurement.[27−29] In comparison, the SWNT bundling morphology (affected by van der Waals attractions) or the presence of carbonaceous coatings are useful results obtained from microscopy measurements.[3] The utility of Raman spectroscopy on the characterization of SWNTs (diameter distribution, electronic type, etc.) is well-established,[30−32] but the complications arising from the use of numerous laser excitation energies in order to resonantly enhance the entire SWNT sample reduce the appeal of this technique as a simple method for the bulk sample analysis of quality or purity.[15] Instead, TGA and optical absorption spectroscopy are the two most prominent methods.[12,13,17,23,29]

Researchers have used TGA to characterize carbon nanotubes for over a decade.[33] It is routinely used to analyze as-produced SWNT samples and purification methods.[23,29] The widespread acceptance and popularity of this method comes from the simplicity of using a representative sample and evaluating the changes in weight loss under flowing gas (typically air) as a function of temperature. Calculation of the metal-catalyst impurity levels is the most routine measurement obtained from TGA,[10,11,23,29,34−43] especially when coupled to an independent method like inductively coupled plasma (ICP) spectroscopy or energy-dispersive X-ray analysis (EDX).[14,15,23,36,39,44,45] However, the TGA only measures a residue value, which means that the proper correction for metal oxidation in raw soot samples is necessary for samples analyzed under flowing air. In addition, the assumption that the residue is equivalent to metal-catalyst impurities alone warrants caution since other contaminants such as SiO_2 may be present in a sample from synthesis and are thermally stable over the SWNT decomposition range.[3] In contrast to quantifying the metal-catalyst content, information regarding the carbonaceous constituents, particularly the SWNT quality (purity) and thermal stability, is less straightforward from TGA data.

TGA has been used to ascribe absolute decomposition temperatures or regions of combustion under flowing air for raw soots and processed SWNTs.[11,12,23,29,40,46−48] The common interpretation for TGA data from raw soot is the presence of two major weight losses attributed to amorphous carbon and SWNTs, respectively, from low (∼300−400 °C) to high temperature (typically > 400 °C).[10,11,28,40,42,49−53] However, the influence of localized exothermic reactions from impurity carbons[27] and/or metal-catalyst oxidation during the decomposition of SWNTs (especially in raw soots) has not always been considered. Numerous reports have identified that precombustion occurs in raw SWNT samples because of thermal oxidation of metal-catalyst impurities.[11,34,39,40,43,54−56] The precombustion effect in raw laser SWNTs has been

(22) Bandow, S.; Rao, A. M.; Williams, K. A.; Thess, A.; Smalley, R. E.; Eklund, P. C. *J. Phys. Chem. B* **1997**, *101*, 8839−8842.
(23) Dillon, A. C.; Gennett, T.; Jones, K. M.; Alleman, J. L.; Parilla, P. A.; Heben, M. J. *Adv. Mater.* **1999**, *11*, 1354−1358.
(24) Jeong, T.; Kim, W.-Y.; Hahn, Y.-B. *Chem. Phys. Lett.* **2001**, *344*, 18−22.
(25) Shi, Z.; Lian, Y.; Liao, F.; Zhou, X.; Gu, Z.; Zhang, Y.; Iijima, S. *Solid State Commun.* **1999**, *112*, 35−37.
(26) Zheng, B.; Li, Y.; Liu, J. *Appl. Phys. A* **2002**, *74*, 345−348.
(27) Kingston, C. T.; Jakubek, Z. J.; Denommee, S.; Simard, B. *Carbon* **2004**, *42*, 1657−1664.
(28) Huang, H.; Marie, J.; Kajiura, H.; Ata, M. *Nano Lett.* **2002**, *2*, 1117−1119.
(29) Rinzler, A. G.; Liu, J.; Dai, H.; Nikolaev, P.; Huffman, C. B.; Rodriguez-Macias, F. J.; Boul, P. J.; Lu, A. H.; Heymann, D.; Colbert, D. T.; Lee, R. S.; Fischer, J. E.; Rao, A. M.; Eklund, P. C.; Smalley, R. E. *Appl. Phys. A* **1998**, *67*, 29−37.
(30) Dresselhaus, M. S.; Dresselhaus, G.; Jorio, A.; Souza Filho, A. G.; Saito, R. *Carbon* **2002**, *40*, 2043−2061.
(31) Jorio, A.; Pimenta, M. A.; Souza Filho, A. G.; Saito, R.; Dresselhaus, G.; Dresselhaus, M. S. *New J. Phys.* **2003**, *5*, 139.1−139.17.
(32) Saito, R.; Gruneis, A.; Samsonidze, G. G.; Brar, V. W.; Dresselhaus, G.; Dresselhaus, M. S.; Jorio, A.; Cancado, L. G.; Fantini, C.; Pimenta, M. A.; Souza Filho, A. G. *New J. Phys.* **2003**, *5*, 157.1−157.15.
(33) Pang, L. S. K.; Saxby, J. D.; Chatfield, S. P. *J. Phys. Chem.* **1993**, *97*, 6941−6942.
(34) Yang, C. M.; Kanoh, H.; Kaneko, K.; Yudasaka, M.; Iijima, S. *J. Phys. Chem. B* **2002**, *106*, 8994−8999.
(35) Chiang, I. W.; Brinson, B. E.; Huang, A. Y.; Willis, P. A.; Bronikowski, M. J.; Margrave, J. L.; Smalley, R. E.; Hauge, R. H. *J. Phys. Chem. B* **2001**, *105*, 8297−8301.
(36) Chiang, I. W.; Brinson, B. E.; Smalley, R. E.; Margrave, J. L.; Hauge, R. H. *J. Phys. Chem. B* **2001**, *105*, 1157−1161.
(37) Landi, B. J.; Ruf, H. J.; Worman, J. J.; Raffaelle, R. P. *J. Phys. Chem. B* **2004**, *108*, 17089−17095.
(38) Lebedkin, S.; Schweiss, P.; Renker, B.; Malik, S.; Hennrich, F.; Neumaier, M.; Stoermer, C.; Kappes, M. M. *Carbon* **2002**, *40*, 417−423.
(39) Moon, J.-M.; An, K. H.; Lee, Y. H.; Park, Y. S.; Bae, D. J.; Park, G.-S. *J. Phys. Chem. B* **2001**, *105*, 5677−5681.
(40) Harutyunyan, A. R.; Pradhan, B. K.; Chang, J.; Chen, G.; Eklund, P. C. *J. Phys. Chem. B* **2002**, *106*, 8671−8675.
(41) Lian, Y.; Maeda, Y.; Wakahara, T.; Akasaka, T.; Kazaoui, S.; Minami, N.; Shimizu, T.; Choi, N.; Tokumoto, H. *J. Phys. Chem. B* **2004**, *108*, 8848−8854.
(42) Furtado, C. A.; Kim, U. J.; Gutierrez, H. R.; Pan, L.; Dickey, E. C.; Eklund, P. C. *J. Am. Chem. Soc.* **2004**, *126*, 6095−6105.
(43) Xu, Y.-Q.; Peng, H.; Hauge, R. H.; Smalley, R. E. *Nano Lett.* **2005**, *5*, 163−168.
(44) Chattopadhyay, D.; Galeska, I.; Papadimitrakopoulos, F. *Carbon* **2002**, *40*, 985−988.
(45) Chiang, I. W.; Brinson, B. E.; Huang, A. Y.; Willis, P. A.; Bronikowski, M. J.; Margrave, J. L.; Smalley, R. E.; Hauge, R. H. *J. Phys. Chem. B* **2001**, *105*, 8297−8301.
(46) Zhang, M.; Yudasaka, M.; Koshio, A.; Iijima, S. *Chem. Phys. Lett.* **2001**, *349*, 25−30.
(47) Zhang, M.; Yudasaka, M.; Koshio, A.; Iijima, S. *Chem. Phys. Lett.* **2002**, *364*, 420−426.
(48) Smith, M. R., Jr.; Hedges, S. W.; LaCount, R.; Kern, D.; Shah, N.; Huffman, G. P.; Bockrath, B. *Carbon* **2003**, *41*, 1221−1230.
(49) Li, H.; Feng, L.; Guan, L.; Shi, Z.; Gu, Z. *Solid State Commun.* **2004**, *132*, 219−224.
(50) Mizoguti, E.; Nihey, F.; Yudasaka, M.; Iijima, S.; Ichihashi, T.; Nakamura, K. *Chem. Phys. Lett.* **2000**, *321*, 297−301.
(51) Murakami, Y.; Miyauchi, Y.; Chiashi, S.; Maruyama, S. *Chem. Phys. Lett.* **2003**, *374*, 53−58.
(52) Hu, H.; Zhao, B.; Itkis, M. E.; Haddon, R. C. *J. Phys. Chem. B* **2003**, *107*, 13838−13842.
(53) Shi, Z.; Lian, Y.; Liao, F. H.; Zhou, X.; Gu, Z.; Zhang, Y.; Iijima, S.; Li, H.; Yue, K. T.; Zhang, S.-L. *J. Phys. Chem. Solids* **2000**, *61*, 1031−1036.
(54) Zimmerman, J. L.; Bradley, R. K.; Huffman, C. B.; Hauge, R. H.; Margrave, J. L. *Chem. Mater.* **2000**, *12*, 1361−1366.

attributed to cobalt-activated decomposition at 425 °C.[36] The verification for this claim occurred by observing the anticipated thermal decomposition below 500 °C after addition of a cobalt salt to purified SWNTs. The exact temperature, extent of weight loss, or impact on TGA peak assignments, however, has yet to be systematically studied for metal activated precombustion of SWNTs.

TGA has been used to investigate the changes in thermal decomposition for samples as a function of SWNT diameter.[11,55,57] The results suggested that smaller-diameter SWNTs decompose at lower temperatures in air based on increased steric strain. Although intuitive, the relationship between the full range of SWNT diameters (typically between 0.4 and 2 nm[1−3]) and thermal decomposition temperatures has not been reported. Raw SWNT soots from synthesis in the same laser vaporization reactor at differing temperatures (resulting in different SWNT diameter distributions) show the expected trend, but consideration for the metal-catalyst precombustion on the results is not discussed.[10] A direct comparison of purified HiPco and laser materials also shows the trend of lower thermal combustion for the smaller-diameter SWNTs,[35] but the diameter distributions are not the only differences between these materials. The effects of metal catalysts from synthesis (Fe vs Ni/Co), type of purification (HCl vs HNO_3), defect densities, and carbonaceous coatings may also contribute to the observed differences in decomposition temperature. The most convincing report for a diameter effect on thermal decomposition involved oxidation treatment at five temperatures (between 460 and 620 °C) on purified HiPco SWNTs.[55] After each successively higher temperature exposure, the authors observed removal of the corresponding higher frequency peaks in the Raman radial breathing mode (RBM), relating to the destruction of smaller-diameter SWNTs.

Reports using TGA to monitor the progress of acid and thermal treatments during SWNT purification processes have been routine for many types of synthesized materials.[23,35,36,39−41,56,58,59] SWNT purification procedures routinely employ chemical, gaseous, and/or thermal oxidation steps to remove metal-catalyst and carbonaceous impurities.[11,12,22−25,28,29,34−36,39−41,43,44,48,50,52,54−70] In general, the observed decomposition temperature during TGA for purified SWNT materials is higher than as-produced, denoting a progressive increase in thermal stability for higher-purity SWNTs.[10,11,23,35,36,39,55] Attempts to quantify SWNT purity for raw and processed SWNTs from TGA data have involved equating SWNT weight percent purity to the entire carbonaceous decomposition change[14,23] or using the ratio of integrated area for the first derivative peaks from curve fitting.[12,28,51,53] This has resulted in high SWNT purity levels being reported from TGA data (up to 98% w/w) without reference to adequate standardization (i.e., reference material or independent technique) or justification for peak area assignments.[14,15,23,27,39,49,53]

Optical absorption spectroscopy has been used for evaluation of SWNT purity, since absorbance is proportional to concentration, and SWNTs exhibit very distinct electronic transitions associated with Van Hove singularities in the density of states.[16−18] The use of SWNT−organic solvent dispersions offers the advantages of quantitative solution-phase analysis and homogeneous sampling without chemical functionalization.[37] Recent work has utilized stable dispersions of SWNTs in *N*,*N*-dimethylacetamide (DMA) for SWNT purity assessment using optical absorption spectroscopy to determine the mass fraction of SWNTs in the carbonaceous portion.[13] The development of constructed sample sets which varied the SWNT mass fraction of purified SWNTs with respect to a representative carbonaceous byproduct allowed for numerous mathematical approaches to be applied in reference to a known metric of comparison. A review of the commonly reported linear subtraction[12,16,52,61,71,72] of the second interband electronic transition of the semiconducting SWNTs ($^{S}E_{22}$) peak showed how this linear approach overestimates the actual SWNT content, supported by both experimental data and a mathematical derivation.[13] Instead, the application of a nonlinear regression model using a Lorentzian subtraction of the π-plasmon, as well as multiple rapid assessment protocols using the $^{S}E_{22}$ and first interband electronic transition of the metallic SWNTs ($^{M}E_{11}$) peak maxima (absolute absorbance intensity, peak maxima ratio, tie-line slope, and a Beer's law analysis derived from calculated extinction coefficients), showed an improved correlation to the constructed sample sets. This report[13] represents the initial example of a calibration standard for SWNT purity, thereby enabling meaningful comparisons with other characterization techniques.

In the present work, a protocol for developing a thermal oxidation profile (TOP) of SWNT-containing samples using

(55) Zhou, W.; Ooi, Y. H.; Russo, R.; Papanek, P.; Luzzi, D. E.; Fischer, J. E.; Bronikowski, M. J.; Willis, P. A.; Smalley, R. E. *Chem. Phys. Lett.* **2001**, *350*, 6−14.
(56) Cinke, M.; Li, J.; Chen, B.; Cassell, A.; Delzeit, L.; Han, J.; Meyyappan, M. *Chem. Phys. Lett.* **2002**, *365*, 69−74.
(57) Nagasawa, S.; Yudasaka, M.; Hirahara, K.; Ichihashi, T.; Iijima, S. *Chem. Phys. Lett.* **2000**, *328*, 374−380.
(58) Strong, K. L.; Anderson, D. P.; Lafdi, K.; Kuhn, J. N. *Carbon* **2003**, *41*, 1477−1488.
(59) Dailly, A.; Yim, J. W. L.; Ahn, C. C.; Miura, E.; Yazami, R.; Fultz, B. *Appl. Phys. A* **2005**, *80*, 717−722.
(60) Gajewski, S.; Maneck, H.-E.; Knoll, U.; Neubert, D.; Dorfel, I.; Mach, R.; Straub, B.; Friedrich, J. F. *Diamond Relat. Mater.* **2003**, *12*, 816−820.
(61) Sen, R.; Rickard, S. M.; Itkis, M. E.; Haddon, R. C. *Chem. Mater.* **2003**, *15*, 4273−4279.
(62) Shen, K.; Curran, S.; Xu, H.; Rogelj, S.; Jiang, Y.; Dewald, J.; Pietrass, T. *J. Phys. Chem. B* **2005**, *109*, 4455−4463.
(63) Tohji, K.; Takahashi, H.; Shinoda, Y.; Shimizu, N.; Jeyadevan, B.; Matsuoka, I.; Saito, Y.; Kasuya, A.; Ito, S.; Nishina, Y. *J. Phys. Chem. B* **1997**, *101*, 1974−1978.
(64) Zhou, O.; Shimoda, H.; Gao, B.; Oh, S.; Fleming, L.; Yue, G. *Acc. Chem. Res.* **2002**, *35*, 1045−1053.
(65) Borowiak-Palen, E.; Liu, X.; Pichler, T.; Knupfer, M.; Graff, A.; Fink, J.; Kalenczuk, R. J.; Jost, O.; Pompe, W. *AIP Conf. Proc.* **2002**, *633*, 341−344.
(66) Bendjemil, B.; Borowiak-Palen, E.; Graff, A.; Pichler, T.; Guerioune, M.; Fink, J.; Knupfer, M. *Appl. Phys. A* **2004**, *778*, 311−314.
(67) Jeong, T.; Kim, W.-Y.; Hahn, Y.-B. *Chem. Phys. Lett.* **2001**, *344*, 18−22.
(68) Coleman, J. N.; O'Brien, D. F.; in het Panhuis, M.; Dalton, A. B.; McCarthy, B.; Barklie, R. C.; Blau, W. J. *Synth. Met.* **2001**, *121*, 1229−1230.
(69) Nepal, D.; Kim, D. S.; Geckeler, K. E. *Carbon* **2005**, *43*, 660−662.
(70) Min, Y. S.; Bae, E. J.; Park, W. *J. Am. Chem. Soc.* **2005**, *127*, 8300−8301.
(71) Hu, H.; Yu, A.; Kim, E.; Zhao, B.; Itkis, M. E.; Bekyarova, E.; Haddon, R. C. *J. Phys. Chem. B* **2005**, *190*, 11520−11524.
(72) Itkis, M. E.; Perea, D. E.; Niyogi, S.; Love, J.; Tang, J.; Yu, A.; Kang, C.; Jung, R.; Haddon, R. C. *J. Phys. Chem. B* **2004**, *108*, 12770−12775.

a systematic series of thermal treatments over the decomposition range for raw and acid-refluxed SWNTs has been performed. The stepwise variation of temperatures allows for a direct comparison of the thermal conditions on SWNT structural and electronic properties, monitored by Raman and optical absorption spectroscopy. Application of the purity assessment method based on a constructed sample set allows for the SWNT purity and mass retention to be calculated after each thermal treatment step. The TOPs of raw soot and acid-refluxed SWNTs show completely different results, which relate to the combustion effects from the metal-catalyst impurities and oxidizing acid exposure. These results facilitate the interpretation of decomposition transitions in the TGA data, including peak assignments in the first derivative analysis. The development of purification calibration curves shows where the delicate relationship between time and temperature on the thermal oxidation of SWNT samples can be used to predict and incorporate systematic thermal treatments to maximize purification efficiency. Such TOP results can allow for larger quantities of purified SWNTs to be retained during purification, as well as can provide a fundamental understanding of SWNT thermal decomposition during TGA.

Experimental Section

The SWNT materials were synthesized by a laser vaporization procedure using an Alexandrite laser.[13,37] The graphite (1−2 μm) target was pressed at 20 000 psi and contained 3% w/w Ni (submicron) and 3% w/w Co (1−2 μm). The reaction furnace temperature was maintained at 1150 °C, with a chamber pressure of 700 Torr under 100 sccm flowing Ar. A portion of the as-synthesized laser raw soot (50 mg) was homogenized for analysis by mixing with 50 mL acetone (reagent grade) and sonicating at 25 °C for 30 min. The solution was magnetically stirred for 30 min and filtered over a 1 μm poly(tetrafluoroethylene) (PTFE) membrane filter. The homogenized raw SWNT paper (raw SWNT-HO) was placed in a muffle furnace under stagnant air (Thermolyne 1300) at 200 °C for 1 h.

The remaining raw SWNT soot was purified by conventional acid reflux as reported previously.[13,23,29,37,42] The ratio of materials for refluxing was as follows: 250 mg raw soot added to the acid solution (150 mL H_2O, 36 mL concentrated HNO_3 (69−70%), and 15 mL concentrated HCl (36.5−38.0%)). The reaction solution was brought to reflux at 120 °C for 14 h. The reflux solution was filtered in three aliquots over a 1 μm PTFE membrane filter with copious distilled H_2O to form SWNT papers. The acid filtrate was discarded and subsequent washes (3x) with 50 mL acetone and 10 mL distilled H_2O removed functionalized carbon impurities until the filtrate was clear. The resulting papers from acid reflux were also thermally oxidized at 200 °C in the muffle furnace under stagnant air for 1 h (SWNT-reflux). The total mass yield of the reflux process was 32% w/w after this step.

Characterization of the raw SWNT-HO and SWNT-reflux materials was performed by scanning electron microscopy (SEM), optical absorption spectroscopy, Raman spectroscopy, and thermogravimetric analysis (TGA). The SEM images were obtained at 2kV using a Hitachi S-900, with samples applied directly to the brass stub using silver paint. UV−Vis−NIR (ultraviolet−visible−near-infrared) spectra were obtained on stable dispersions of SWNTs in *N*,*N*-dimethylacetamide (DMA, 99+ %) using a Perkin-Elmer Lambda 900 spectrophotometer.[37] Sample handling for dispersion solutions involved the use of 1 cm quartz cuvettes. Data were obtained over an energy range of 0.90−4.25 eV, corresponding to the transmission window of the alkyl amide solvent. Raman spectroscopy was performed at room temperature using a JY-Horiba Labram spectrophotometer from 100 to 3000 cm^{-1} with an excitation energy of 1.96 eV (He/Ne laser). Thermogravimetric analysis (TGA) was conducted using a TA Instruments 2950. Samples were placed in the platinum pan balance in quantities of ∼1 mg and ramped at 10 °C/min from room temperature up to 800 °C under air at a gas flow rate of 60 sccm.

The purity assessment was performed as per the previous report using a constructed sample set which was fabricated from 3.25 μg/mL DMA dispersions and prescribed as the reference standard.[13] This was accomplished by a volumetric mixture of a 3.25 μg/mL stock solution of purified laser SWNTs in DMA with a 3.25 μg/mL stock solution of nanostructured carbon (NC) in DMA at 10% increments (i.e., concentrations of 0%, 10%, 20%, 30%, 40%, 50%, 60%, 70%, 80%, 90%, and 100% w/w SWNTs). However, it should be noted that the choice of carbon impurities will affect the constructed sample sets. Selection of NC is a suitable material since it was manufactured in the same laser synthesis reactor under equivalent conditions as the SWNTs except for the lack of metal catalyst in the graphite target.[13]

Thermal oxidation profiling (TOP) was performed by thermally oxidizing representative fractions of the SWNT samples at a given temperature and duration, followed by calculation of the corresponding mass change and SWNT purity[13] from such treatment. Each measurement was performed using the TGA for accurate reproduction of the temperature ramp and microbalance measurements. The procedure involved ramping ∼1 mg samples (accurate mass measured by instrument) in the TGA at 10 °C/min to the desired temperature and stopping or holding isothermally for predetermined times. The change in mass was calculated by the TGA, and purity assessment of the remaining material proceeded as per the reported protocol.[13] A more complete discussion of the calculations used to determine each of the SWNT mass retention data points in the TOP will be provided in part C of the Results and Discussion section.

Results and Discussion

A. SWNT Purity Assessment. As per the previous report,[13] a constructed sample set was prepared by volumetric mixing of stock DMA dispersions of purified SWNTs (denoted as "100%") with the respective carbon impurity constituent: nanostructured carbon (NC). Figure 1 displays the characteristic optical absorption data for the DMA dispersions from a laser SWNT constructed sample set at carbonaceous concentrations of 3.25 μg/mL (adjusted for the decomposition residue values from the TGA data), which is near the dispersion limit for purified SWNTs.[37] The current sample set is at a higher dispersion concentration and contains twice as many data points (10% intervals) than the

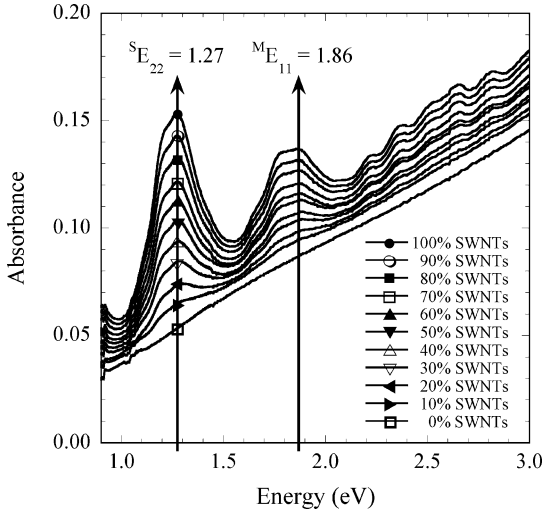

Figure 1. Optical absorption data for a laser SWNT constructed sample set for 3.25 μg/mL DMA dispersions at the various SWNT weight fraction percentages.

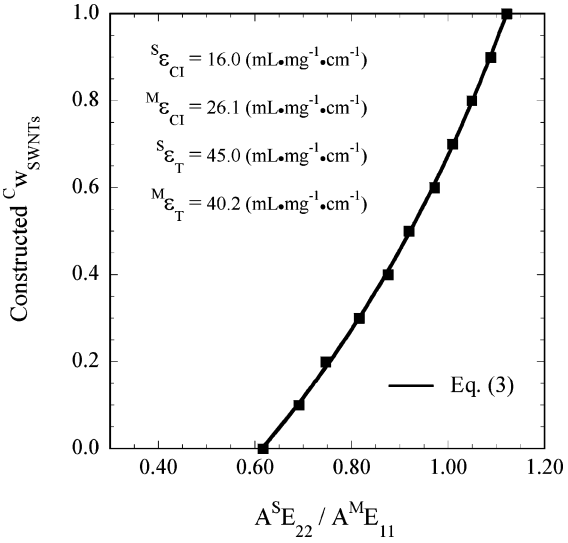

Figure 2. Purity assessment calibration curve for the ratio of absorbance values at the $^{S}E_{22}$ and $^{M}E_{11}$ peak maxima (as designated by the arrows in Figure 1.). The solid curve-fit line represents application of eq 3 to the data, and the corresponding fitting parameters are listed.

previous report[13] to enhance the accuracy of the calibration curve. The figure depicts the well-resolved peaks (e.g., $^{S}E_{22}$ at 1.27 eV and $^{M}E_{11}$ at 1.86 eV) due to the interband electronic transitions in the density of states for SWNTs.[73] The overall absorption in each SWNT-containing sample fraction is a superposition of absorbances due to the interband electronic transitions and background π-plasmons of the respective amounts of SWNTs and carbon impurities. The dramatic change in absorption intensity as a function of SWNT mass fraction in the carbonaceous portion of the sample ($^{c}w_{SWNTs}$) provides the necessary reference standard for a purity-assessment calibration curve.

The most attractive method for rapid evaluation of SWNT purity in a sample is the calculation of the absorbance maxima ratio from the $^{S}E_{22}$ peak and $^{M}E_{11}$ peak.[13] The ratio of peak maxima for a pure SWNT sample result is a convolution of the purity with the semiconducting/metallic ratio (S/M) and the ratio of extinction coefficients for the semiconducting and metallic types.[13] For a sample of unknown purity, the absorption spectrum will represent the absorbance contribution from the SWNT chirality distribution and carbon impurities present. If the S/M and extinction coefficients for pure SWNTs are assumed to remain constant and nonvarying during the experiment, then the ratio of peak maxima directly relates to the change in concentration of SWNTs to carbon impurities. Selection of peak maxima values for purity assessment has important advantages over integrated area based on the observed SWNT distribution in a laser-synthesized sample. For the $^{S}E_{22}$ and $^{M}E_{11}$ peaks shown in Figure 1, the superposition of interband electronic transitions based on the sample's diameter range gives rise to the amplitude being proportional to the area with minimal effects of peak overlap and the ambiguous selection of integration limits. Therefore, the present SWNT purity assessment is performed using the peak maxima values at 1.27 eV ($^{S}E_{22}$) and 1.86 eV ($^{M}E_{11}$) for the establishment of a calibration curve.

The resulting absorbance peak maxima ratio values for the constructed sample set from Figure 1 are plotted in Figure 2. The preparation of the constructed SWNT mass fractions, $^{c}w_{SWNTs}$, was calculated to have an experimental uncertainty of 1.5% based on sample weighing and the volumetric pipets. The absorbance ratio error is negligible due to the accuracy and precision of the spectrometer. In contrast to the previous work where the peak maxima ratio data was approximated with a linear dependence, the closer-spaced data intervals (10%) in Figure 2 allow for a more accurate curve fit of the data. Whether the data is analyzed using an empirical relationship for the peak maxima ratio or by applying measured extinction coefficient values (as suggested in the previous work[13]), the relationship using the absorbance peak maxima for purity assessment is equivalent. The changes in the absorbance maxima ratio depict the weighted contributions of each carbonaceous component's extinction coefficient on the overall magnitude of the peaks. The SWNTs have very pronounced intensities at the selected peaks in comparison to the carbonaceous impurities (purified SWNTs have ~3x the extinction coefficient as the representative carbon impurities in the form of NC[13,37]). Therefore, the extent of SWNT contribution will directly correspond to the observed changes in absorbance peak maxima ratio, as described in the following derivation:

The absorbance (A) of an SWNT-containing DMA dispersion at either the $^{S}E_{22}$ or $^{M}E_{11}$ peak is equal to the extinction coefficient of the dispersion (ϵ_D) multiplied by the concentration of the dispersion (c_D) for a constant path length (see eq 1). (The $^{S}E_{22}$ peak is represented by the superscript S, and the $^{M}E_{11}$ peak is represented by the superscript M.) The extinction coefficient of the dispersion, ϵ_D, represents a weighted contribution from the extinction coefficients of the SWNTs (ϵ_T) and carbon impurities (ϵ_{CI}) present, with the weighting based on the mass fraction of each, ϕ_T and ϕ_{CI}, respectively.

$$\frac{^{S}A}{^{M}A} = \frac{^{S}\epsilon_D c_D}{^{M}\epsilon_D c_D} \equiv \frac{^{S}\epsilon_D}{^{M}\epsilon_D} \equiv \frac{[^{S}\epsilon_T\phi_T + {}^{S}\epsilon_{CI}\phi_{CI}]}{[^{M}\epsilon_T\phi_T + {}^{M}\epsilon_{CI}\phi_{CI}]} \qquad (1)$$

(73) Kataura, H.; Kumazawa, Y.; Maniwa, Y.; Umezu, I.; Suzuki, S.; Ohtsuka, Y.; Achiba, Y. *Synth. Met.* **1999**, *103*, 2555−2558.

The major advantage of using the absorbance peak maxima ratio for purity assessment, aside from the simplicity, is that it is dispersion-concentration independent (as is evident by eq 1), provided the DMA dispersion is below the purified SWNT dispersion limit. With rearrangement, the ratio of mass fractions for SWNTs to carbon impurities (ϕ_T/ϕ_{CI}) is the following:

$$\frac{\phi_T}{\phi_{CI}} = \frac{\left[{}^{S}\epsilon_{CI} - {}^{M}\epsilon_{CI}\left(\frac{{}^{S}A}{{}^{M}A}\right)\right]}{\left[{}^{M}\epsilon_{T}\left(\frac{{}^{S}A}{{}^{M}A}\right) - {}^{S}\epsilon_{T}\right]} \quad (2)$$

The mass fraction of SWNTs in the carbonaceous material, ${}^{c}w_{SWNTs}$, results in the following:

$${}^{c}w_{SWNTs} = \frac{\left(\frac{\phi_T}{\phi_{CI}}\right)}{\left[1 + \left(\frac{\phi_T}{\phi_{CI}}\right)\right]} \equiv \frac{\left[{}^{S}\epsilon_{CI} - {}^{M}\epsilon_{CI}\left(\frac{{}^{S}A}{{}^{M}A}\right)\right]}{\left[{}^{M}\epsilon_{T}\left(\frac{{}^{S}A}{{}^{M}A}\right) - {}^{S}\epsilon_{T}\right] + \left[{}^{S}\epsilon_{CI} - {}^{M}\epsilon_{CI}\left(\frac{{}^{S}A}{{}^{M}A}\right)\right]} \quad (3)$$

Although a simple quadratic approximation can be used to fit the data (with an $R^2 > 0.999$) in Figure 2, the appropriate calibration curve is based on application of the physically based Beer's Law ratio function, eq 3. Therefore, purity assessment during the present work will be based on the calibration curve generated from eq 3, and represented as the solid line ($R^2 = 0.9996$) in Figure 2. The curve-fit parameters (calculated using the general curve fit in the KaleidaGraph software package) are the extinction coefficients of carbon impurities and SWNTs at each peak maximum. The values extracted from the curve fit are the following: ${}^{S}\epsilon_{CI} = 16.0$ (mL·mg^{-1}·cm^{-1}); ${}^{M}\epsilon_{CI} = 26.1$ (mL·mg^{-1}·cm^{-1}); ${}^{M}\epsilon_{T} = 40.2$ (mL·mg^{-1}·cm^{-1}); and ${}^{S}\epsilon_{T} = 45.0$ (mL·mg^{-1}·cm^{-1}). Previous work has experimentally determined the value of the extinction coefficients for NC and purified laser-SWNT−DMA dispersions at the ${}^{S}E_{22}$ and ${}^{M}E_{11}$ peaks using a Beer's law analysis from concentration dilutions.[13,37] The self-consistency between the curve-fitted values and the experimental extinction coefficient values (within 3%) is a testament to the quality of the constructed sample set and the utility of eq 3 for purity assessment. It is important to note that overlap of SWNT electronic transitions can influence any experimentally calculated ϵ, but the value derived from selecting the peak maximum will be the least sensitive to this effect. The use of calculated extinction coefficients from a different SWNT sample maintains the aforementioned assumption that SWNT samples being analyzed have a similar S/M, since the magnitude of the extinction coefficient values are a convolution of the extinction properties with the inherent S/M.[13]

B. Material Characterization. To ensure proper measurement accuracy and reproducibility, characterization of SWNT-containing samples must be performed on representative portions of a homogeneous sample. Since the laser vaporization process produces raw soot with a random mixture of SWNTs and synthesis byproducts, it is imperative as a first step prior to characterization of the raw soot to homogenize the materials. In the present case, a solution process is utilized whereby the raw soot is mixed with acetone and sonication, magnetic stirring, and filtration are performed to produce the homogenized raw soot (raw SWNT-HO). The efficacy of this procedure was investigated with five representative portions for analysis using TGA and optical absorption spectroscopy. The designation of "homogenized" was given to samples when experimental data between portions overlaid to within a standard deviation of 1%. For raw soot which undergoes the acid-reflux step (SWNT-reflux), it is not necessary to pre-homogenize, since this step produces homogenized materials in the process. This assertion is based upon results from the same analysis criteria on five portions of a SWNT-reflux paper.

The use of an acid reflux as the initial step in the purification of raw laser SWNT soot is quite common.[23,29] The removal of the metal-catalyst impurities (Ni, Co, etc.) by dilute mineral acids is well-known,[74] and control over the chemical oxidation process on SWNT quality through reflux time has been investigated.[23] The acid-reflux process promotes acid intercalation into the SWNT bundles,[75,76] with the resulting effects of SWNT debundling in solution, facilitating a uniform chemical exposure.[62] This process promotes chemical oxidization of the carbonaceous components (both the impurities and the defect sites on the SWNTs).[23,42] The chemical functionalization of carbon impurities is highly advantageous for subsequent removal, but surface functionalization (chemical oxidation) and chemical doping of the SWNTs can also occur in the presence of these conditions.[42,77,78] However, these effects are not problematic since post-reflux thermal-treatment steps have been shown to remove intercalated acid and oxygenated functional groups on SWNTs.[23,42]

In the present case, a conventional acid-reflux step was employed, including a subsequent solvent washing to remove functionalized carbon impurities. The acid reflux consisted of a mixture of dilute HNO_3 and HCl to enhance the oxidizing effects and solubility of both nickel and cobalt metal catalysts.[74] The oxidized carbon impurities were removed with alternating acetone−H_2O washes. The efficiency of the process (mass retention and purity) can be calculated from purity assessment of the raw soot and refluxed samples with the corresponding mass yield after the purification steps. Shown in Figure 3 are the optical absorption data for 3 μg/mL DMA dispersions of raw SWNT-HO and SWNT-reflux samples. The purified SWNT sample ("100%" from the constructed sample set) is overlaid in the figure for comparison. Using eq 3, the calculated ${}^{c}w_{SWNTs}$ is 19% for raw SWNT-HO and 59% for SWNT-reflux. Given the mass yield of 32% w/w after the acid reflux,

(74) Greenwood, N. N.; Earnshaw, A. *Chemistry of the Elements*; Pergamon Press Ltd.: New York, 1984.
(75) Bower, C.; Kleinhammes, A.; Wu, Y.; Zhou, O. *Chem. Phys. Lett.* **1998**, *288*, 481−486.
(76) Martinez, M. T.; Callejas, M. A.; Benito, A. M.; Cochet, M.; Seeger, T.; Anson, A.; Schreiber, J.; Gordon, C.; Marhic, C.; Chauvet, O.; Maser, W. K. *Nanotechnology* **2003**, *14*, 691−695.
(77) Monthioux, M.; Smith, B. W.; Burteaux, B.; Claye, A.; Fischer, J. E.; Luzzi, D. E. *Carbon* **2001**, *39*, 1251−1272.
(78) Hennrich, F.; Wellmann, R.; Malik, S.; Lebedkin, S.; Kappes, M. M. *Phys. Chem. Chem. Phys.* **2003**, *5*, 178−183.

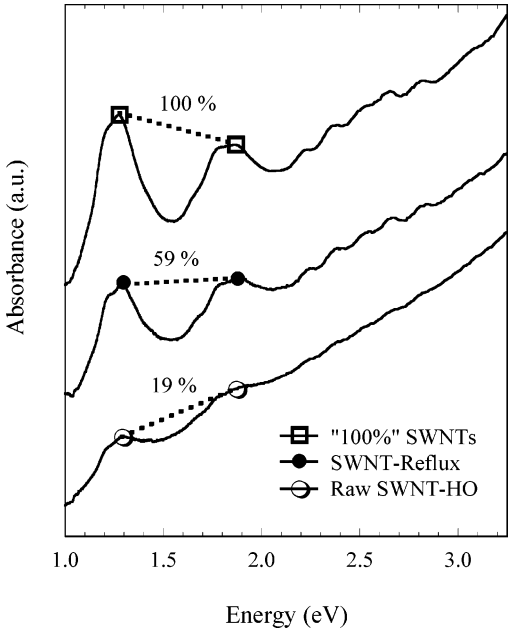

Figure 3. Optical absorption data for 3 μg/mL DMA dispersions of raw SWNT-HO (○) and SWNT-reflux (●) samples in comparison to the "100%" sample from the constructed sample set (□). The calculated ${}^{c}w_{SWNTs}$ using eq 3 for the raw SWNT-HO and SWNT-reflux are listed as 19% and 59% w/w, respectively. The peak maxima tie lines illustrate the relative changes in absorption due to the sample purity. The data are offset in the *y*-axis for clarity.

solvent wash, and sample drying at 200 °C, there is nearly 100% w/w retention of the SWNTs after these purification steps. This result is in contrast to some nitric acid purification reports on arc-produced SWNTs which cite SWNT destruction from similar acid-reflux conditions[52,71] and is attributed to the quality of laser-produced raw soot.[15]

As a comparison, the ${}^{c}w_{SWNTs}$ of an SWNT paper from acid reflux without the acetone−H_2O washing is 21% w/w, which reflects a slight increase in carbonaceous purity over the raw soot. This result is supported by the clear differences in filtrate color and composition for the two filtration steps. During the standard acid-reflux filtration, the filtrate is amber in color, which is attributed in part to the dissolved metal catalyst but is mostly due to functionalized carbon impurities (NC acid refluxed under the same conditions without the presence of any metal catalysts showed the same color). However, the acetone wash produces a turbid-black filtrate which shows identical optical absorption characteristics to the NC materials, thus indicating removal of carbonaceous impurities.

The morphological changes in the raw soot from the acid reflux−acetone wash steps can be qualitatively evaluated using SEM. Shown in Figure 4 are representative SEM images of the (a) raw SWNT-HO and (b) SWNT-reflux samples. The typical morphology of amorphous carbon and metal-catalyst impurities mixed with the SWNT bundles is observed in the raw SWNT-HO sample. The SWNT material after the acid reflux and acetone wash shows a significantly improved morphology as seen in Figure 4b. The presence of entangled SWNT bundles, with only trace metal catalyst and significantly reduced carbon impurities, is clearly observed.

The Raman spectra for the raw SWNT-HO and SWNT-reflux samples are obtained from a 1.96 eV (He/Ne laser)

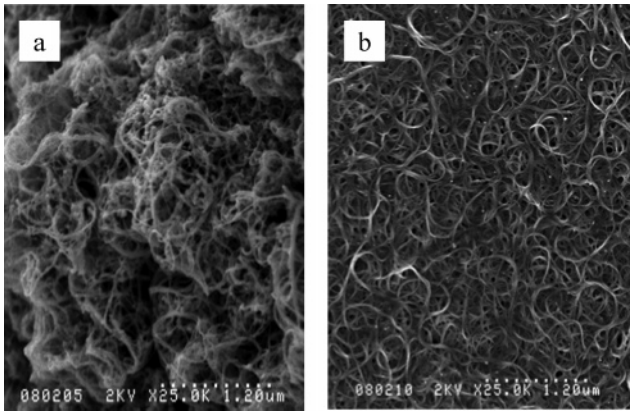

Figure 4. SEM images of (a) raw SWNT-HO and (b) SWNT-reflux samples at a magnification of 25 000×.

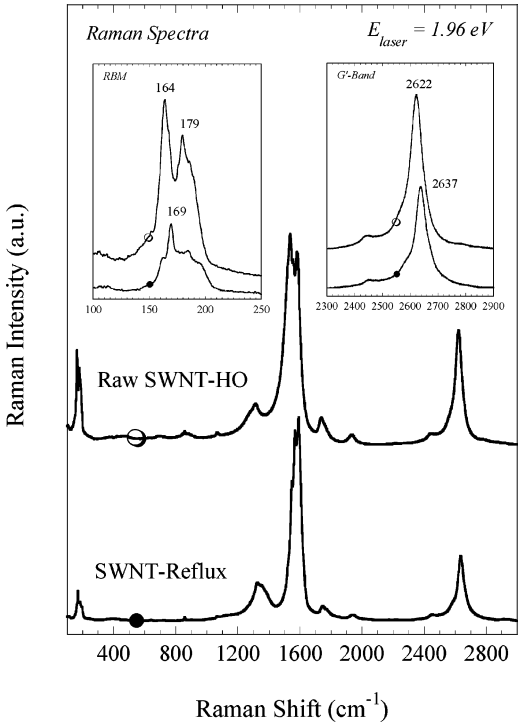

Figure 5. Raman spectra for raw SWNT-HO (○) and SWNT-reflux (●) samples at a laser excitation energy of 1.96 eV. The inset overlays depict the radial breathing mode (RBM) region from 100 to 250 cm^{-1} and the G′-band region from 2300 to 2900 cm^{-1}. The spectra are offset in the *y*-axis, and peak values are labeled for clarity.

excitation and are depicted in Figure 5. The characteristic spectrum for laser raw SWNT soot is apparent with the RBM range of 140−200 cm^{-1} (corresponding to a diameter range of 1.2−1.5 nm for bundled SWNTs[79]). The D-band at ∼1320 cm^{-1} originates from multiple resonance effects, arising from SWNT defects or carbonaceous impurities.[32,80] The G-band ranges from ∼1350−1600 cm^{-1} and is composed of two components from symmetry-allowed vibrations in the SWNT axial (denoted as G^+ at ∼1590 cm^{-1}) and circumferential (denoted as G^- over the range of ∼1350−1550 cm^{-1}, with an SWNT electronic-type dependence on the line shape) directions.[81,82] The present G^- data displays the broad

(79) Rao, A. M.; Chen, J.; Richter, E.; Schlecht, U.; Eklund, P. C.; Haddon, R. C.; Venkateswaran, U. D.; Kwon, Y.-K.; Tomanek, D. *Phys. Rev. Lett.* **2001**, *86*, 3895−3898.
(80) Dillon, A. C.; Parilla, P. A.; Alleman, J. L.; Gennett, T.; Jones, K. M.; Heben, M. J. *Chem. Phys. Lett.* **2005**, *401*, 522−528.

asymmetric Breit−Wigner−Fano (BWF) line shape (because of discrete phonon coupling to a continuum of electron density) for resonantly enhanced metallic SWNTs.[83,84] The G′-band observed at 2622 cm^{-1} results from a two-phonon scattering which is explained by double resonance theory and is known to be highly sensitive to the density of electronic states for the resonantly enhanced SWNTs.[32,81,85]

Comparison of the Raman spectra for raw SWNT-HO and SWNT-reflux samples (Figure 5) indicates several pronounced effects from the purification step (acid reflux−acetone wash). The data for the RBM and G′-band are highlighted by the insets in Figure 5. Nitric acid exposure on SWNTs is notorious for modifying the Raman spectra due to charge-transfer effects, which alters the electronic density of states.[42,57,62,76,86,87] This effect is manifested in relative Raman intensity quenching and peak upshifts (shifts to higher corresponding frequencies). The quenching of the SWNT-reflux Raman intensity in comparison to the raw SWNT-HO is evident for the RBM (factor of 3), relative to the G^+-band intensity. The RBM in the SWNT-reflux also shows a slight upshift in the observed peak maximum at 169 cm^{-1} compared to the corresponding raw soot value at 164 cm^{-1}. The D-band between samples shows minor peak changes, but the general peak position and structure (sharp underlying SWNT peak and a broad amorphous carbon peak) is consistent with recent work.[80] The G^+-band peak shifts from 1583 cm^{-1} in the raw SWNT-HO to 1591 cm^{-1} in the SWNT-reflux. The prominent G^- mode, indicative of the BWF line shape observed in the raw SWNT-HO, is significantly quenched during the acid-reflux step, consistent with charge transfer from the metallic SWNTs.[84,87] The G′-band also shows a relative intensity quenching (factor of 2), in relation to the G^+-band, for SWNT-reflux as compared to the raw SWNT-HO. The most prominent upshifts, however, are observed in the G′-band peak (from 2622 to 2637 cm^{-1}), which appears to be highly sensitive to acid-doping effects.

The TGA data for raw SWNT-HO and SWNT-reflux samples under 60 sccm flowing air and a ramp rate of 10 °C/min are compared in Figure 6. The initial decrease in mass for the SWNT-reflux sample below 300 °C is typical of residual acid and adsorbed water in the sample.[23] The change in TGA residue at 800 °C is also apparent in Figure 6a, with the average from five analyses listed for the raw SWNT-HO (9.6% w/w) and SWNT-reflux (7.1% w/w). In both samples, the residue value constitutes the metal oxide present, except for the possibility of other thermally stable

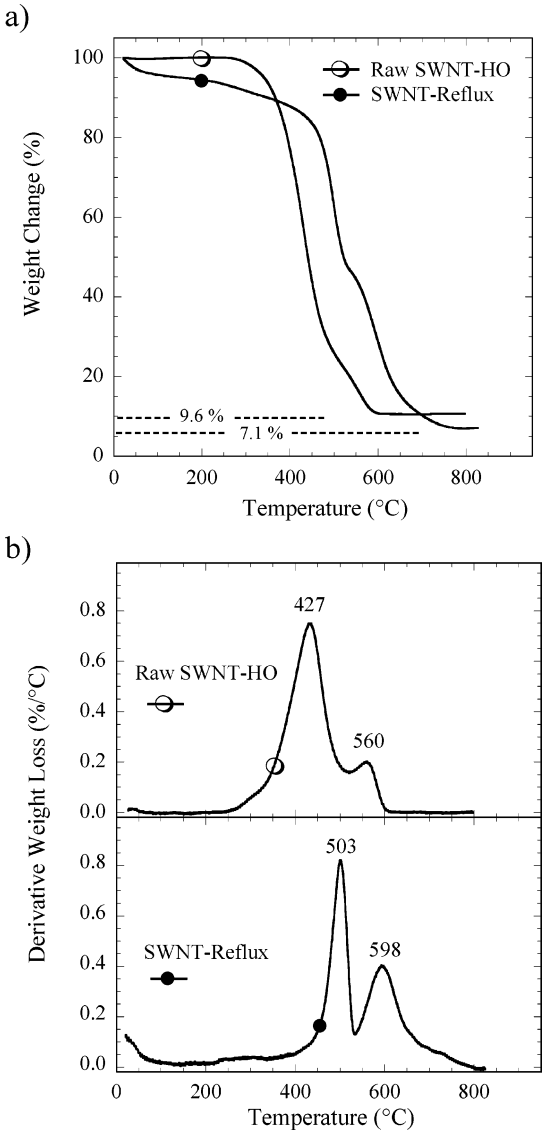

Figure 6. (a) TGA data for raw SWNT-HO (○) and SWNT-reflux (●) samples. The TGA was ramped at 10 °C/min for each thermogram under 60 sccm flowing air. The average residue from five analyses is listed for each sample, determined at 800 °C. (b) TGA data from the first derivative analysis of the weight loss (%/°C) for raw SWNT-HO (○) and SWNT-reflux (●) samples. The peak maxima for the prominent thermal-decomposition features are labeled for clarity.

synthesis impurities (such as SiO_2).[3] Since the raw soot contains pure metal from laser synthesis, the TGA is thermally oxidizing the metal particles. The actual % w/w metal impurities in the raw soot is calculated using an adjustment for the oxidation process (relative mass is calculated assuming Ni/Co metal is 76% of the TGA residue value for a 50:50 mixture and oxidation to NiO and Co_3O_4). In the case of the SWNT-reflux sample, there should be complete (or partial if encapsulated metal catalysts are present) chemical oxidation by the acid, resulting in metal oxides in the acid-refluxed sample. Then, the actual % w/w impurities in SWNT-reflux are already metal oxide and are equivalent to the measured TGA residue.

Most purification steps involve an acid or thermal process to oxidize the metal-catalyst impurities for removal. Therefore, it is convenient to interpret the TGA data in a way that the relative fraction of metal oxide to SWNTs can be calculated and the subsequent metal-catalyst removal can be

(81) Dresselhaus, M. S.; Dresselhaus, G.; Jorio, A.; Souza Filho, A. G.; Saito, R. *Carbon* **2002**, *40*, 2043−4061.
(82) Jorio, A.; Pimenta, M. A.; Souza Filho, A. G.; Saito, R.; Dresselhaus, G.; Dresselhaus, M. S. *New J. Phys.* **2003**, *5*, 139.1−139.17.
(83) Brown, S. D. M.; Jorio, A.; Corio, P.; Dresselhaus, M. S.; Dresselhaus, G.; Saito, R.; Kneipp, K. *Phys. Rev. B* **2001**, *63*, 155414.
(84) Rao, A. M.; Eklund, P. C.; Bandow, S.; Thess, A.; Smalley, R. E. *Nature* **1997**, *388*, 257−259.
(85) Souza Filho, A. G.; Jorio, A.; Swan, A. K.; Unlu, M. S.; Goldberg, B. B.; Saito, R.; Hafner, J. H.; Lieber, C. M.; Pimenta, M. A.; Dresselhaus, G.; Dresselhaus, M. S. *Phys. Rev. B* **2002**, *65*, 085417.
(86) Zhang, X.; Sreekumar, T. V.; Liu, T.; Kumar, S. *J. Phys. Chem. B* **2004**, *108*, 16435−16440.
(87) Zhou, W.; Vavro, J.; Nemes, N. M.; Fischer, J. E.; Borondics, F.; Kamaras, K.; Tanner, D. B. *Phys. Rev. B* **2005**, *71*, 205423.

monitored. The mass fraction of metal oxide to SWNTs (${}^{s}w_{MO}$) will reflect the change in TGA residue in relation to the ${}^{c}w_{SWNTs}$. For the raw SWNT-HO sample, the calculated ${}^{s}w_{MO}$ is 50% w/w since the ${}^{c}w_{SWNTs}$ is 19% and the TGA residue is 9.6%. After acid reflux, the ${}^{s}w_{MO}$ improves to 12% w/w given the fact that the ${}^{c}w_{SWNTs}$ has increased to 59% w/w. Although the acid-reflux step shows a lower TGA residue value, the more important metric for SWNT purification is the reduction in ${}^{s}w_{MO}$, which reflects the removal of metal-catalyst impurities in relation to SWNTs.

The other major trend between samples is the progression to a higher decomposition temperature for the SWNT-reflux material. This is demonstrated in Figure 6b by the first derivative weight-loss curves for each sample. The raw SWNT-HO data reflects two major transitions with the prominent peak maximum at 427 °C and a minor shoulder at 560 °C. The common interpretation for this type of raw-soot TGA data is that the transitions are attributed to amorphous carbon and SWNTs, respectively, from low (~300−400 °C) to high temperature (typically > 400 °C).[10,11,28,40,42,49−53] In addition, some groups have tried to infer purity levels from evaluating the integrated area of the first derivative peaks using multiple Lorentzian curve fitting.[12,28,51,53] The ability to identify independent regions of combustion for SWNTs and carbon impurities (if they exist) would be extremely advantageous to purity assessment and purification monitoring. However, there has been no verification of the specific temperature or range of temperatures in which SWNT decomposition solely occurs. Furthermore, the effects of metal-catalyzed precombustion, especially in the raw soot, have not been fully considered. The SWNT-reflux data also show two major transitions, but shifted to higher temperatures, namely, peak maxima at 503 and 598 °C, respectively. The acid-reflux results are similar to previous work, in which the authors cited the lower-temperature transition to functionalized carbon impurities and the higher-temperature transition to SWNTs.[23] There are similarities between the TGA data, but material tolerance to thermal exposure is clearly different.

C. Thermal Oxidation Profiling (TOP). The general idea of thermal oxidation profiling (TOP) is to monitor any changing properties of SWNT samples at incremental intervals over a prescribed temperature range. In the present work, the establishment of a TOP during thermal decomposition of raw and acid-refluxed samples is performed. Each sample measurement is conducted by using ~1 mg of the SWNT-containing sample in the TGA and ramping from 25 °C at 10 °C/min under 60 sccm flowing air to the desired temperature and stopping or holding isothermally for a desired duration. In the case of raw SWNT-HO, the temperature range is 250−525 °C, at 25 °C intervals. For the SWNT-reflux sample, the temperature range is 250−575 °C, with 50 °C intervals from 250 to 400 °C and then 25 °C intervals to 575 °C.

The current TOP consists of two data sets: (1) the calculated SWNT mass fraction of SWNTs in the carbonaceous material, ${}^{c}w_{SWNTs}$, and (2) the corresponding SWNT mass retention (R) in each sample. After each thermal treatment, a portion of the remaining sample is dispersed in DMA at 3 μg/mL (below the dispersion limit), and ${}^{c}w_{SWNTs}$ is calculated using the purity assessment protocol established in part A of the Results and Discussion section. The SWNT mass retention (R) represents the ratio of SWNT mass remaining after thermal treatment $(m_{SWNTs})_r$ in relation to the original mass of SWNTs in the sample $(m_{SWNTs})_o$.

$$R = \frac{(m_{SWNTs})_r}{(m_{SWNTs})_o} \tag{4}$$

The mass of SWNTs is equal to the weight fraction of SWNTs in the carbonaceous material, ${}^{c}w_{SWNTs}$, multiplied by the total carbonaceous mass in both the original (o) and retained (r) samples.

$$(m_{SWNTs})_o = (m_{carbonaceous})_o({}^{c}w_{SWNTs})_o \tag{5}$$

$$(m_{SWNTs})_r = (m_{carbonaceous})_r({}^{c}w_{SWNTs})_r \tag{6}$$

The original SWNT-containing sample mass $(m_{sample})_o$ is a sum of both the carbonaceous material $(m_{carbonaceous})_o$ and the metal-catalyst oxide residue $(m_{metal})_o$.

$$(m_{carbonaceous})_o = (m_{sample})_o - (m_{metal})_o \tag{7}$$

During the TOP, the TGA measures the weight change from the thermal oxidation of the carbonaceous materials. The mass of carbonaceous material retained $(m_{carbonaceous})_r$ is determined by subtracting the mass of carbonaceous material thermally oxidized during treatment $(m_{carbonaceous})_t$ and the metal-catalyst oxide residue $(m_{metal})_o$ from the original sample mass $(m_{sample})_o$.

$$(m_{carbonaceous})_r = (m_{sample})_o - (m_{carbonaceous})_t - (m_{metal})_o \tag{8}$$

Thus, R can be represented by the following:

$$R = \frac{[(m_{sample})_o - (m_{carbonaceous})_t - (m_{metal})_o]({}^{c}w_{SWNTs})_r}{[(m_{sample})_o - (m_{metal})_o]({}^{c}w_{SWNTs})_o} \tag{9}$$

In the case of purification procedures, the TOP data can also be presented in the form of the purification efficiency (PE) at each thermal oxidation step:

$$\mathrm{PE} = (R)({}^{c}w_{SWNTs})_r \tag{10}$$

The original mass is measured by the TGA instrument microbalance, and the weight change is analyzed upon completion of the temperature profile. The mass of metal oxide is based on the average value determined previously from five sample measurements to determine homogeneity (i.e., 9.6% w/w for raw SWNT-HO and 7.1% w/w for SWNT-reflux). Given the experimental uncertainty of 1.5% for the purity assessment procedure and homogenization error for TGA data (1.0%), the experimental uncertainty for calculated SWNT mass retention values is propagated to be 2.5%.[88]

D. TOP of Raw SWNT Soot. The TOP for raw SWNT-HO samples (~1 mg) is shown in Figure 7 and corresponds to data obtained after a thermal ramp at 10 °C/min to each temperature. The SWNT mass retention (R) is relatively constant until ~350 °C, where the values begin to sharply

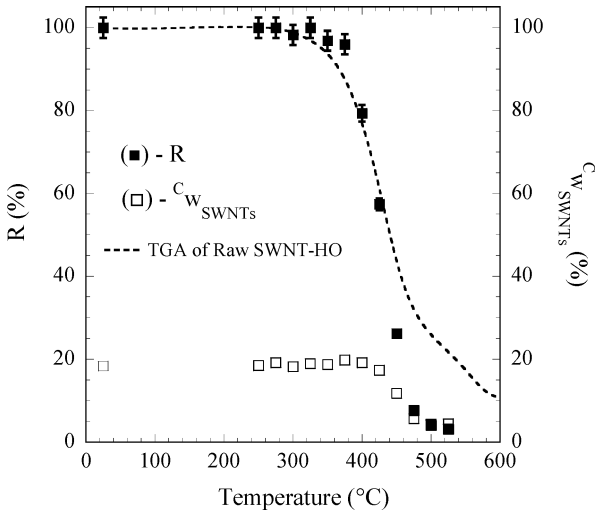

Figure 7. Thermal oxidation profile (TOP) for raw SWNT-HO depicting the SWNT mass retention, *R*, (■) and SWNT weight fraction in the carbonaceous material, $^{c}w_{SWNTs}$, (□) as a function of temperature treatment (i.e., ramp 10 °C/min to temperature-stop and then analyze). The dashed line represents the TGA data for raw SWNT-HO (with the corresponding *y*-axis label being weight change (%) as in Figure 6a).

decrease. The general trend in $^{c}w_{SWNTs}$ is constant purity to ~400 °C and then a steady decline to <5% at 525 °C. The dashed line in Figure 7 is the TGA thermogram for raw SWNT-HO (with the corresponding *y*-axis label being weight change (%) as in Figure 6a). Thus, the TOP indicates that the onset of decomposition for the SWNTs is nearly equivalent to the overlaying TGA curve. The TOP shows ~50% destruction of SWNTs by ~425 °C, which is comparable to the peak maximum at 427 °C in the TGA first derivative weight-loss curve of raw SWNT-HO in Figure 6b. Therefore, the results imply that the first major transition in a thermogram of raw soot contains the thermal decomposition of the SWNTs. The SWNTs are almost entirely decomposed by 500 °C. The shoulder at a higher temperature is not significantly enriched with SWNTs but is due to remaining carbonaceous impurities. Purified laser SWNTs are reported to decompose at ~770 °C.[13] Therefore, the lower-temperature decomposition (peaked at ~425 °C) in the raw SWNT-HO sample is presumably due to an interaction of SWNTs with other constituents remaining from synthesis.

These TOP results are supported by the Raman data for each sample after temperature treatment. Shown in Figure 8 is the RBM at representative temperature intervals. The general trend is a constant diameter distribution with no apparent peak shifts until 450 °C. Then, the relative peak intensities exhibit an attenuation of the corresponding higher-frequency peaks, indicating removal of smaller SWNT diameters from the distribution. The progressive thermal

(88) It should be noted that analysis of raw soot actually has the underlying oxidation of metal-catalyst impurities convolved with the carbonaceous material oxidation. Since the extent of metal-catalyst oxidation is varying throughout the decomposition range, subtraction by the total residue value will estimate the total effects of metal oxidation on any weight change increase. Therefore, this assumption will underestimate the value of *R* until the temperature at which equivalent metal oxidation has occurred with the residue value. However, this correction factor is still less at any given point than the experimental uncertainty of 2.5% established for the current TOP technique.

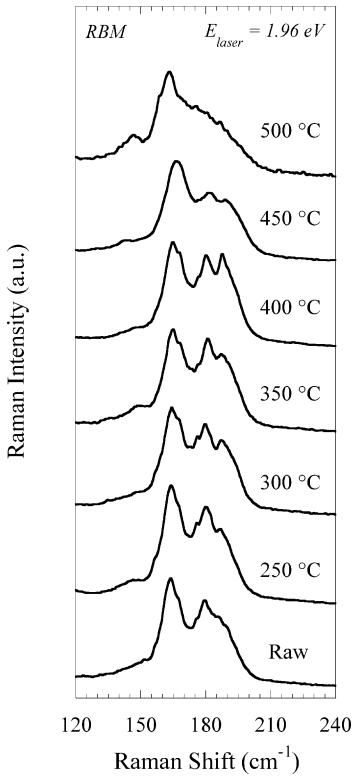

Figure 8. Raman data at select temperature intervals for raw SWNT-HO samples in the region of the radial breathing mode (RBM) at a laser excitation energy of 1.96 eV. The effects of the thermal oxidation on removal of the higher frequency peaks (i.e., smaller-diameter SWNTs) is observed at higher temperatures.

increment to 500 °C shows the continued trend toward higher thermal stability for larger-diameter SWNTs, as has been suggested previously.[55] The changes in the diameter distribution correlated with the observed $^{c}w_{SWNTs}$ trend in the TOP, which depicts the gradual decrease in SWNT content above 400 °C. Further evidence for this trend comes from Figure 9, which evaluates the D- and G-bands of the raw SWNT-HO sample at representative temperature intervals for the TOP. Again there are no apparent shifts in any peak positions, but the obvious trend is the increase in relative intensity of the D-band to the G^{+}-band. This ratio is qualitatively used to evaluate the defect content or fraction of carbon impurities present in a SWNT sample.[3,32,80] The significant enhancement in the D/G ratio at 500 °C is attributed to a decrease in SWNT content and/or disruption of the structural integrity for SWNTs present. Overall, evaluation of both the TOP and Raman data suggests that there is no temperature range during thermal oxidation in raw soot which is solely due to SWNT combustion and independent of impurity influence.

The concurrence between the onset of decomposition for raw SWNT-HO and the decrease in *R* is a result of the underlying mechanism for thermal oxidation in these samples. Shown in Figure 10 are the first derivative weight-loss curves for raw SWNT-HO in comparison with nanostructured carbon (NC) and the pure metal catalysts used during synthesis (Ni and Co). The similarity in thermal decomposition for NC and the shoulder in the raw SWNT-HO are consistent with the observation in the raw soot TOP for carbonaceous impurities of comparable morphology to be

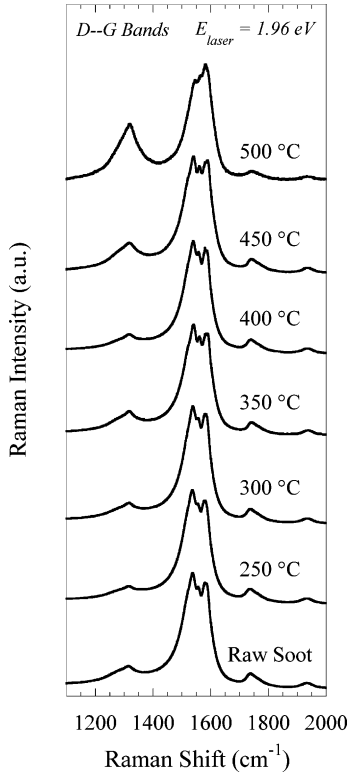

Figure 9. Raman data for raw SWNT-HO samples at select temperature intervals in the region of the D- and G-Bands at a laser excitation energy of 1.96 eV. The progressive increase in the D/G relative intensity ratio from the thermal oxidation treatment at higher temperature is apparent.

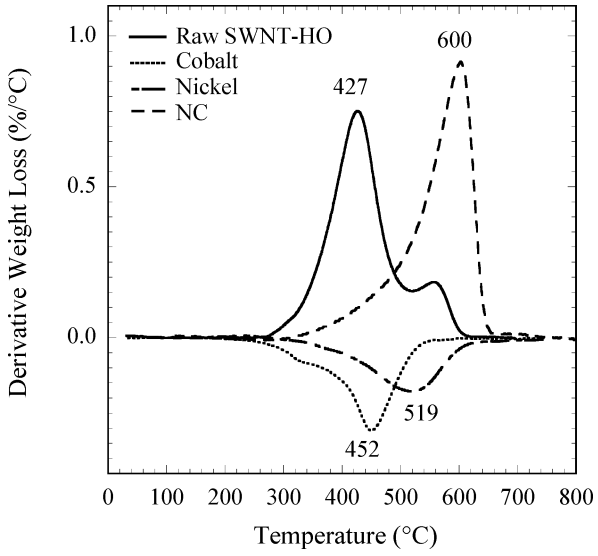

Figure 10. TGA first derivative analysis of the weight loss (%/°C) for raw SWNT-HO in comparison to cobalt metal catalyst (<2 μm), nickel metal catalyst (submicron), and nanostructured carbon (NC). The TGA was ramped at 10 °C/min for each thermogram under 60 sccm flowing air. The temperature equivalence for onset of thermal decomposition between raw SWNT-HO and Co metal-catalyst oxidation is clearly shown.

stable above 500 °C. Evident from the data is the temperature equivalence in thermal oxidation for the pure metal catalysts, particularly Co and raw SWNT-HO. It is suggestive, then, that the global oxidation for raw soot inferred from the TOP data is initiated by metal-catalyst oxidation reactions at these temperatures.

The combustion of raw SWNT soot is typical of various carbon allotropes mixed with metal oxides, especially in an overoxidized, flowing air environment.[89,90] It is well-known that catalytic gasification of carbon by O_2 and metals lowers the carbon decomposition by several hundred degrees, depending on the metal.[89] In the present case, the incorporation of pure metal catalysts in the raw SWNT soot further promotes catalytic gasification. The onset of thermal oxidation at ~300 °C for pure Co metal to form the stable solid oxide, Co_3O_4, and pure Ni metal to form the stable solid oxide, NiO, is observed in Figure 10. The reported heats of formation (ΔH_f) for these oxides at 25 °C is −213 kcal/mol and −57.3 kcal/mol, respectively.[91] The exothermicity of these reactions is more than sufficient to initiate thermal oxidation of the carbonaceous components (given that reported activation energies for graphitized carbon oxidation are typically small, 6.4 kcal/mol[89]). Propagation of the carbon combustion can occur by additional metal-catalyst oxidation and the formation of CO(g) and CO_2(g) ($\Delta H_f = -26.4$ kcal/mol and −94.0 kcal/mol, respectively). This mechanism is consistent with exothermic reactions where the transition state energy is near the energy of the starting materials (i.e., Hammond's Postulate).[92] Furthermore, it is reasonable to assume that Co and Ni atoms bound directly to the SWNT backbone (which are observed by TEM prevalently in the literature[62,77,93]) will catalytically lower the energetic transition state for carbon oxidation and initiate localized combustion.[89] These results are in agreement with the recent discussion involving raw soot combustion initiated by light.[94,95]

The raw soot TOP is consistent with the previous suggestion that the global oxidation of raw soots at lower temperature (~300−500 °C) is insufficient at purifying the materials to an appreciable level.[40] Unfortunately, many groups have utilized low-temperature oxidations in air (from 250 to 470 °C) as an initial step in the purification process for raw soots.[19,36,39,42,53,58,60,61,63] However, the prospect of thermally removing non-SWNT carbon without activating the metal-catalyst oxidation is improbable based on the current TOP results. Removal of the metal-catalyst impurities is deemed to be paramount to a high SWNT purification efficiency. Therefore, purification approaches which are selective to the metal (both bound catalyst particles and catalyst particles being encapsulated within a carbonaceous shell) are very important to develop. Alternative purification treatments to "crack" the encapsulated metal particles, such as microwave heating,[40] alkali metal intercalation,[59] and alkyl radicals,[96] may offer tremendous potential given the estab-

(89) Kinoshita, K. In *Carbon: Electrochemical and Physicochemical Properties*; John Wiley & Sons: New York, 1988; pp 174−195.
(90) Stanmore, B. R.; Brilhac, J. F.; Gilot, P. *Carbon* **2001**, *39*, 2247−2268.
(91) *Handbook of Chemistry and Physics*, 71st ed.; CRC Press: Boca Raton, FL, 1990.
(92) Lowry, T. H.; Richardson, K. S. In *Mechanism and Theory in Organic Chemistry*, 3rd ed.; Harper & Row Publishers: New York, 1987; pp 212−214.
(93) Alvarez, W. E.; Kitiyanan, B.; Borgna, A.; Resasco, D. E. *Carbon* **2001**, *39*, 547−558.
(94) Ajayan, P. M.; Terrones, M.; de la Guardia, A.; Huc, V.; Grobert, N.; Wei, B. Q.; Lezec, H.; Ramanath, G.; Ebbesen, T. W. *Science* **2002**, *296*, 705.
(95) Bockrath, B.; Johnson, J. K.; Sholl, D. S.; Howard, B.; Matranga, C.; Shi, W.; Sorescu, D.; Ajayan, P. M.; Ramanath, G.; Terrones, M.; Ebbesen, T. W. *Science* **2002**, *297*, 192−193.

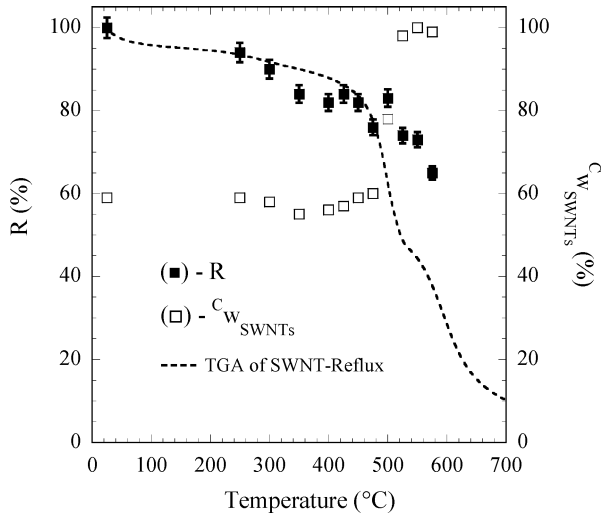

Figure 11. Thermal oxidation profile (TOP) for SWNT-reflux depicting the SWNT mass retention, *R*, (■) and SWNT weight fraction in the carbonaceous material, $^{c}w_{SWNTs}$, (□) as a function of temperature treatment (i.e., ramp 10 °C/min to temperature-stop and then analyze). The dashed line represents the TGA data for SWNT-reflux (with the corresponding *y*-axis label being weight change (%) as in Figure 6a).

lished metric for comparison. On the basis of the raw soot TOP, the commonly accepted view that SWNT-containing samples will always decompose in the order of amorphous carbon impurities first and then SWNTs is shown to be incorrect. The misconception, although relevant to raw SWNT soot, may not be applicable to processed materials such as acid-refluxed samples which have completely different sample morphology and potentially different thermal oxidation profiles.

E. TOP of Acid-Refluxed SWNTs. Investigation of the SWNT-reflux TOP is displayed in Figure 11 for data obtained after a thermal ramp at 10 °C/min to each temperature for the SWNT-reflux samples (~1 mg). The SWNT mass retention (*R*) shows minor fluctuations but ultimately retains ~65% SWNTs at 575 °C. The dashed line in Figure 11 is the TGA thermogram for SWNT-reflux (with the corresponding *y*-axis label being weight change (%) as in Figure 6a). The lack of correlation between *R* and the thermogram for SWNT-reflux indicates that a different thermal oxidation mechanism exists for the SWNT-reflux sample. The $^{c}w_{SWNTs}$ shows a minor decrease in purity, ~5% from 300 to 400 °C, but the most striking change is between 475 and 525 °C, where the sample purity changes from ~60% to >90% over the span of 50 °C. The inflection point for the $^{c}w_{SWNTs}$ data occurs at the first transition's peak maximum in the SWNT-reflux first derivative weight-loss data (see Figure 6b). Therefore, the drastic increase in SWNT purity occurs after the lower-temperature peak in the first derivative data is nearly removed. This result on purity for SWNT-reflux is in contrast to that for raw SWNT-HO; although both samples showed very similar first derivative curves, just SWNT-reflux is shifted to a slightly higher temperature. Therefore, simple inspection of first derivative curves is very ambiguous for a qualitative interpretation of the decomposition mechanism and SWNT purity, especially without prior knowledge of specific purification conditions.

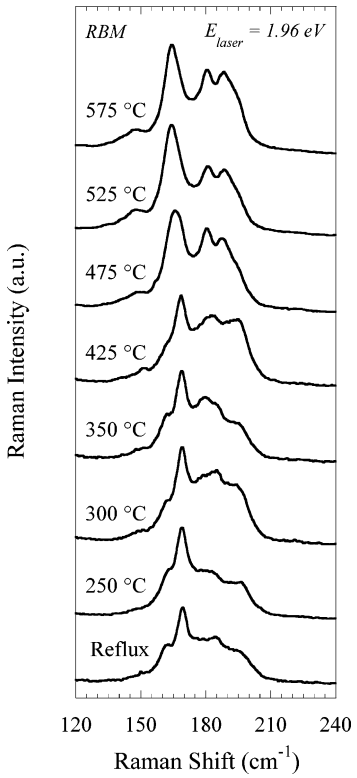

Figure 12. Raman data for SWNT-reflux samples at select temperature intervals in the region of the radial breathing mode (RBM) at a laser excitation energy of 1.96 eV. The restoration of the RBM intensity and peak downshift at higher temperature is observed.

Analysis of the thermal treatment intervals on the Raman modes can provide a direct probe of the doping effects from variations in SWNT electronic states.[35,42,44,62,86,87,97] The corresponding peak frequencies and degrees of shifts for acid-exposed SWNT samples will be sensitive to the acid content and degree of intercalated species present, in turn providing a purification monitor for removal. Shown in Figure 12 are the RBMs at representative temperature intervals from the TOP for SWNT-reflux samples. The restoration of the RBM features after high-temperature treatment (400−500 °C) is consistent with previous work.[42,57,62,76,86] The prominent peak at 169 cm^{-1} in the SWNT-reflux begins downshifting during the thermal treatment, initially at 450 °C, with a convergence to 164 cm^{-1} at thermal exposures >500 °C. The corresponding peak frequencies for the RBM and other major Raman modes at each temperature interval in the SWNT-reflux TOP are listed in Table 1. The RBM distribution for the 575 °C sample is from 140 to 200 cm^{-1}, which corresponds to the equivalent range of SWNT diameters observed in the raw SWNT-HO. Although in some instances nitric acid processing has been reported to remove smaller-diameter SWNTs,[36,86] in the present case the diameter distribution during the acid-reflux process is tolerant to the acid and thermal conditions. This result is not surprising, given that the predominant diameter distribution for the laser SWNTs synthesized in this work is calculated to be from 1.2−1.5 nm[13] and the previous

(96) Sadana, A. K.; Liang, F.; Brinson, B. E.; Arepalli, S.; Farhat, S.; Hauge, R. H.; Smalley, R. E.; Billups, W. E. *J. Phys. Chem. B* **1005**, *109*, 4416−4418.

(97) Itkis, M. E.; Niyogi, S.; Meng, M. E.; Hamon, M. A.; Hu, H.; Haddon, R. C. *Nano Lett.* **2002**, *2*, 155−159.

Table 1. Raman Peak Frequencies (±1 cm^{-1} for the Major Modes at 1.96 eV Excitation) of the SWNT-Reflux TOP Samples in Comparison to Raw SWNT-HO

sample	RBM (cm^{-1})	D-band (cm^{-1})	G$^+$-band (cm^{-1})	G′-band (cm^{-1})
SWNT-reflux	169	1326	1591	2637
reflux − 250 °C	169	1324	1591	2635
reflux − 300 °C	169	1324	1591	2635
reflux − 350 °C	169	1324	1591	2634
reflux − 400 °C	169	1323	1591	2633
reflux − 425 °C	169	1323	1591	2632
reflux − 450 °C	169	1323	1590	2631
reflux − 475 °C	166	1321	1590	2628
reflux − 500 °C	164	1319	1587	2625
reflux − 525 °C	164	1319	1585	2622
reflux − 550 °C	164	1318	1583	2622
reflux − 575 °C	164	1317	1583	2622
raw SWNT-HO	164	1315	1583	2622

results on HiPco materials[86] showed that SWNTs with diameters ≤1 nm were digested with dilute HNO_3 solutions.

The effects of the thermal treatments on the D- and G-bands for the SWNT-reflux sample are shown in Figure 13. The narrowing in the D-band structure is obvious at higher-temperature treatments, which illustrates the progressive removal of the broad amorphous carbon peak underlying the relatively sharp SWNT feature. The peak for the D-band also downshifts from the SWNT-reflux value (1326 cm^{-1}) to approximately the same corresponding frequency as the raw SWNT-HO for the sample treated at 575 °C (see Table 1). The slight offset in D-band peak position between raw SWNT-HO (1315 cm^{-1}) and the high purity sample after 575 °C (1317 cm^{-1}) is attributed to the removal of underlying carbonaceous impurities, which is superposed with the raw

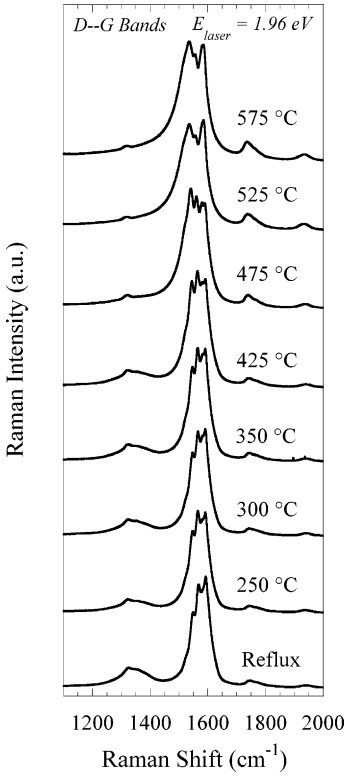

Figure 13. Raman data for SWNT-reflux samples at select temperature intervals in the region of the D- and G-bands at a laser excitation energy of 1.96 eV. The decrease in D/G relative intensity ratio and restoration of the BWF line shape for the G$^-$ band is apparent with higher-temperature treatment.

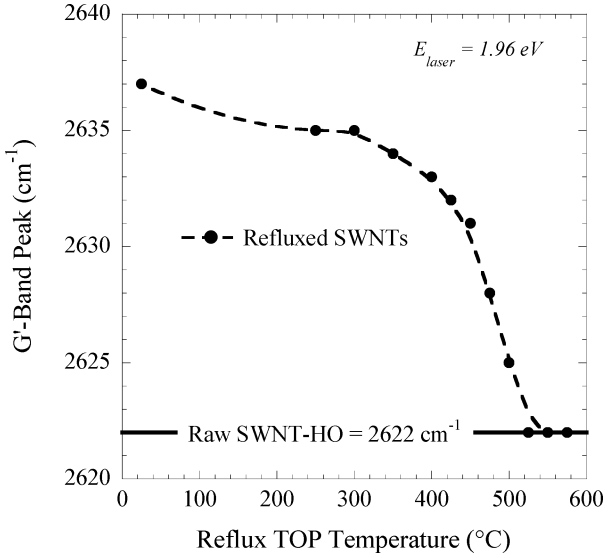

Figure 14. G′-band peak position in the Raman data from a laser excitation energy of 1.96 eV for SWNT-reflux samples at designated temperature intervals from the thermal oxidation profile (TOP). The dashed line represents a weighted trendline through the data points for visual clarity. The solid line indicates the G′-band peak position of raw SWNT-HO at 2622 cm^{-1}.

SWNT-HO peak (the D-band peak for NC is at 1308 cm^{-1}). The G-band displays two major changes during the thermal treatments to higher temperature, namely, restoration of the BWF line shape for the G$^-$ peak and the downshift in the G$^+$ peak (see Table 1). The effects of SWNT bundling are not expected to explain such changes in the G-band,[98] since all samples are analyzed from the same solid paper where the bundling state was predetermined from the filtering step. Rather, these changes are simply due to the removal of acid and the corresponding doping effects on the SWNT-reflux sample.

The most prominent Raman mode affected by acid-induced charge-transfer effects is the G′-band peak. The corresponding peak frequencies at each temperature interval are listed in Table 1 and plotted in Figure 14. The increase in temperature progressively downshifts the G′-band in the SWNT-reflux sample. The inflection point in Figure 14 occurs at ∼475 °C, which also corresponds to the temperature where each of the other Raman modes (RBM, D, and G) begin downshifting from the acid-doped peak position. The eventual convergence of the G′-band peak frequency to 2622 cm^{-1}, equal to the raw SWNT-HO, represents the undoped state. Therefore, thermal treatments from a ramp of 10 °C/min to 500 °C are required to fully remove acid from the reflux process. This assertion is consistent with recent work on SWNT-templated ordering of acid molecules in the SWNT bundles which render higher stability.[99] The acid-doping results are not proposed to be purity dependent, since purified SWNT papers exposed to HNO_3 show reversible doping effects upon heating. Therefore, the corresponding peak frequency of the G′-band is a highly sensitive probe to doping effects in SWNTs and can be used to monitor acid doping from the reflux process.

(98) Bendiab, N.; Almairac, R.; Paillet, M.; Sauvajol, J.-L. *Chem. Phys. Lett.* **2003**, *372*, 210−215.
(99) Zhou, W.; Heiney, P. A.; Fan, H.; Smalley, R. E.; Fischer, J. E. *J. Am. Chem. Soc.* **2005**, *127*, 1640−1641.

The dramatic difference in TOP results for SWNT-reflux compared to raw SWNT-HO is attributed primarily to chemical oxidation of the metal-catalyst impurities. However, there is an observed decrease in purity from 300 to 400 °C in the SWNT-reflux sample. This is possibly due to residual metal-catalyst impurities that were either encapsulated during the reflux process or only partially oxidized by the acid. The effects of intercalated acid and carbonaceous coatings on the electronic transitions of SWNTs are also well-known.[42,57,62,76,86,87] Therefore, the calculated ${}^{c}w_{SWNTs}$ for the SWNT-reflux sample may be affected by such interactions at lower temperatures, but acid effects become mitigated with progressively higher thermal treatment. During the reflux, the acid can react with occluded carbon impurities while intercalating into SWNT bundles to exfoliate individual SWNTs and attack carbonaceous coatings. The known effects of carbonaceous functionalization also contribute to the change in thermal oxidation behavior between raw SWNT-HO and SWNT-reflux samples.[23] Acid oxidation of carbon impurities is well-known to form surface oxide groups which lower the thermal stability.[89] As observed in the TOP, the removal of such impurities at lower temperature is complemented by the rapid increase in SWNT purity at temperatures higher than 475 °C.

F. Purification Monitoring of Acid-Refluxed SWNTs. The TOP analysis of SWNT-reflux shows where the functionalized carbon impurities oxidize preferentially at a lower temperature than the SWNTs. In fact, at temperatures above 475 °C, the SWNT purity rapidly increases to levels comparable to the "100%" reference sample in the constructed sample set while maintaining a mass retention of ~65% w/w. Therefore, the TOP analysis implies that optimization of the thermal treatments (time, temperature, ramp rate,[11] etc.) will have a dramatic effect on the SWNT retention efficiency. Since most thermal steps in purification procedures involve an isotherm at a designated temperature, an understanding of how the exposure time influences the resulting ${}^{c}w_{SWNTs}$ and R is important. Figure 15 depicts R for SWNT-reflux samples that were all ramped at 10 °C/min with the isotherm time at each temperature being varied (from stop, 30 min, and 60 min). The value of R is independent of isotherm time until ~400 °C, when there is a divergence between the ramp-stop and the isotherm samples. The separation in R continues as the samples approach 550 °C between a ramp-stop (~65% w/w), compared to the two isothermal exposures (~35% w/w). The difference in R is ~30% w/w and illustrates the delicate balance between the thermodynamics and kinetics of combustion in the SWNT-reflux sample, particularly in the temperature region near the first major decomposition transition (refer to Figure 6b). The corresponding ${}^{c}w_{SWNTs}$ for each TOP data point at differing isotherms is shown in Figure 16. The decrease in purity from 300 to 400 °C is observed in each of the isothermal treatments, albeit the effect is lessened with longer isotherm time. Each of the isotherm conditions converges at the 100% purity level, although the inflection point decreases to a lower temperature for the longer isotherm times (by more than 100 °C). The rapid increase in SWNT purity is observed in each of the samples

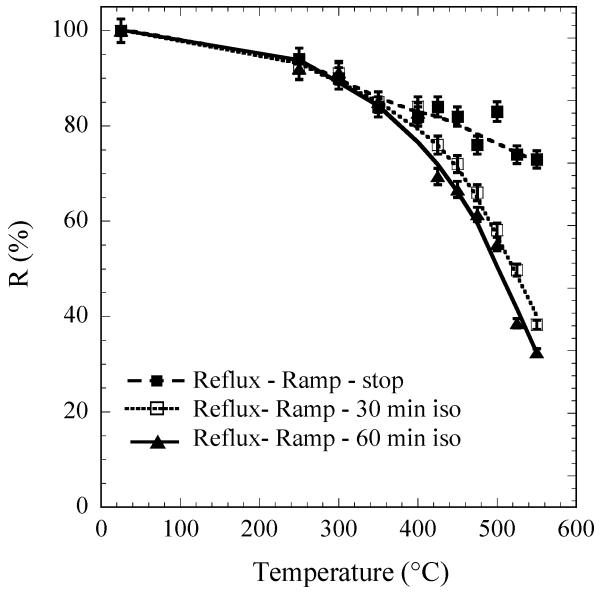

Figure 15. SWNT mass retention, R, data for SWNT-reflux samples under differing isotherm conditions after the 10 °C/min ramp to temperature. The weighted trendlines are shown through the data points for clarity.

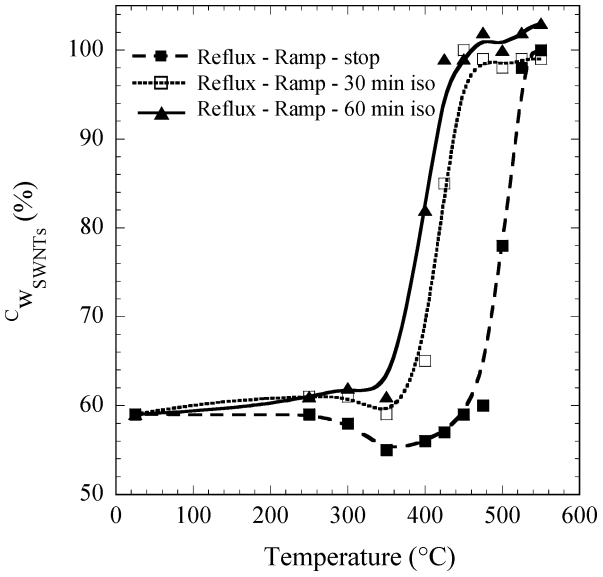

Figure 16. SWNT weight fraction in the carbonaceous material, ${}^{c}w_{SWNTs}$ (%), data for SWNT-reflux samples under differing isotherm conditions after the 10 °C/min ramp to temperature. The weighted trendlines are provided for clarity. The experimental uncertainty for these data is 1.5%; however, the error bars are omitted for clarity.

with similar rates of purity change, indicating a transition state that is dependent on both temperature and time.

The TOP data can also be expressed in terms of the purification efficiency (PE), which is designated by eq 10 and depicted in Figure 17 for each of the isotherm conditions. Attempts to establish a purification efficiency are not new,[14,15,23,29,36,41,52,61,71] but the use of a purity-assessment method[13] relying on standards from a constructed sample set is unique to the present analysis. The present PE value reflects the quality of SWNTs (maximum percentage of SWNTs at the highest purity) for a given purification procedure. The general shifts in SWNT purity inflection temperature observed in Figure 16 are manifested in the corresponding PE maxima in Figure 17 over a similar range of ~100 °C, depending on the isotherm time. Ultimately,

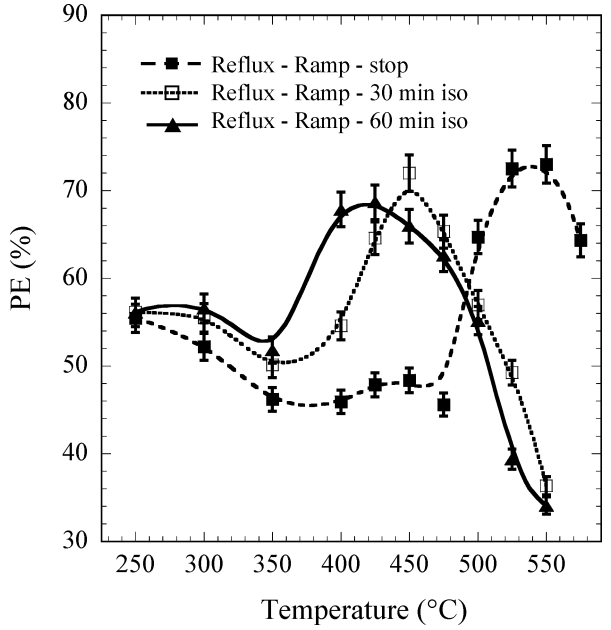

Figure 17. SWNT purification efficiency, PE, data for SWNT-reflux samples under differing isotherm conditions after the 10 °C/min ramp to temperature. The weighted trendlines are shown through the data points for clarity.

the ramp-stop data features the maximum PE of ~73% w/w between 525 and 550 °C. This PE value represents the benchmark for these purification conditions and can be used as a metric of comparison for alternative purification steps. In the current set of isotherm data, the PE assesses the most appropriate combination of time and temperature for a given ramp rate of 10 °C/min under 60 sccm flowing air. As mentioned earlier, the acid-reflux process employed currently retains nearly 100% of the SWNTs from the raw soot. Given a PE of 73% for the ramp-stop at 525 °C, the net result is 73% of the SWNTs synthesized during the laser vaporization process are retained with purity equal to 100% of the reference standard.

G. Kinetics of Thermal Oxidation in Acid-Refluxed SWNTs. Previous attempts to model the kinetics of SWNT combustion utilized SWNT samples containing metal-catalyst impurities, thus rendering the results suspect based on the precombustion effects.[60,100] The SWNT-reflux paper represents bundles of SWNTs with ~40% carbonaceous impurities, in the predominant form of carbonaceous coatings based on SEM and TEM. Therefore, isothermal treatment of SWNT-reflux is expected to result in combustion initiation at dangling sp^3 hybridized bonds and surface oxides with propagation to the carbonaceous coatings. The surface exothermic reactions will produce CO(g) and CO_2(g) simultaneously, which can propagate combustion that etches away the carbonaceous coatings. It is proposed that the combustion proceeds from the periphery inward to the SWNT bundles, since the high SWNT thermal conductivity prevents thermal runaway and the enhanced order in an SWNT bundle (i.e., the close-packed array of tubes) promotes higher thermal stability. Future verification of the kinetic mechanism for SWNT-reflux combustion should be possible through appropriate modeling of isotherm data.

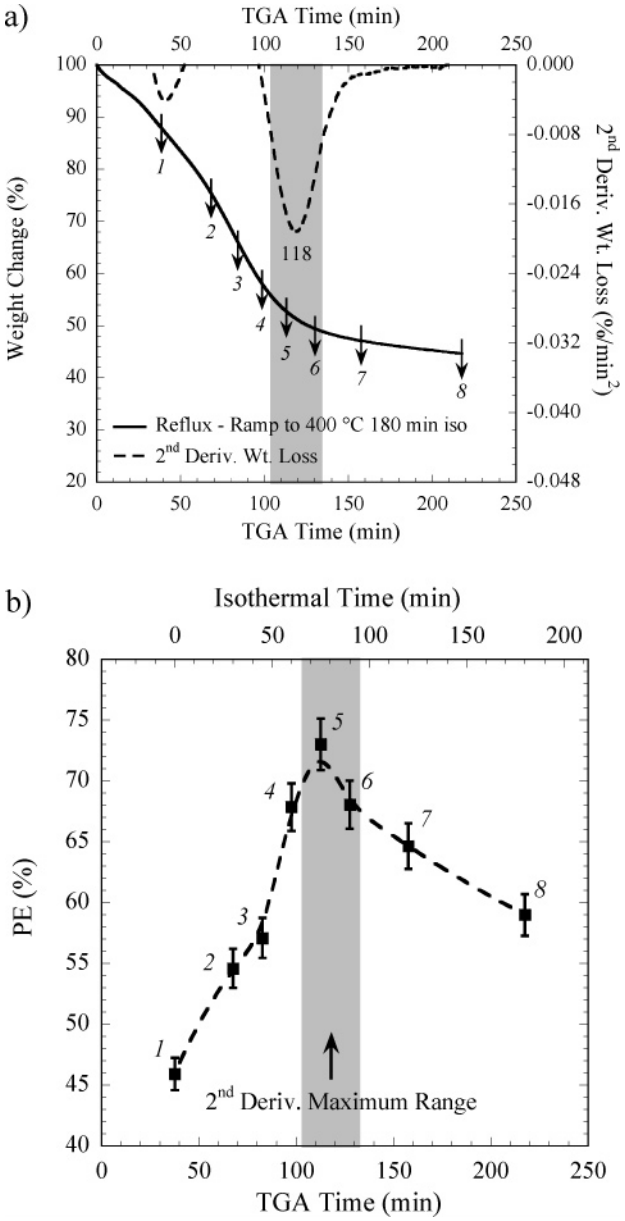

Figure 18. (a) TGA thermogram for a SWNT-reflux sample ramped at 10 °C/min to 400 °C and held isothermal for 180 min. The second derivative of the weight loss is represented by the dashed line with the peak minimum labeled and the TGA time range depicted by the gray box. The arrowed numbers represent samples at select time intervals for analysis as shown in (b), where the effect of isothermal time treatment on the SWNT purification efficiency, PE, is determined. The weighted trendline through the data points is shown for clarity. The similarity between the apparent PE maximum and the second derivative minimum is illustrated by the equivalent gray box.

The results from the purification monitoring show a delicate balance of time and temperature on the SWNT combustion and resultant purity. The ability to utilize kinetic control during the purification process prompted a further investigation of isotherm time on the PE. Selection of an appropriate temperature for isothermal treatment is based on a thermal level where the PE varies with isotherm time (refer to Figure 17) and also at a point in the decomposition profile such that the temperature is high enough for combustion (refer to Figure 6b). Therefore, 400 °C is a suitable candidate, particularly since the onset of the major transition in the first

(100) Illekova, E.; Csomorova, K. *J. Therm. Anal. Calorim.* **2005**, *80*, 103–108.

derivative weight loss occurs at this temperature (Figure 6b). The isothermal TGA curve at this temperature is shown in Figure 18a and depicts the weight change for an isotherm time of 180 min (total TGA time of ~220 min includes the ramp from room temperature to 400 °C). Attempts to model the isotherm data in Figure 18a show that the combustion kinetics for SWNT-reflux samples contain multiple reaction steps and various reaction orders, as would be expected from such a sample. Sample aliquots were taken after thermal treatment at isotherm times of 30, 45, 60, 75, 90, 120, and 180 min (represented by the arrowed numbers in the figure). The PE for these samples is depicted in Figure 18b and indicates a relative maximum at the 75 min isotherm sample (TGA time of 113 min) with a total PE approaching 75% w/w. This region of maximum PE corresponds to the second derivative weight-loss curve minimum at 118 min in Figure 18a, represented by the gray-shaded box in both parts a and b of Figure 18. The effects of isotherm time, however, are entirely dependent on the temperature. A similar kinetic measurement at 350 °C required 720 min to show an equivalent weight-change plateau in the SWNT-reflux sample, as observed at ~45% w/w in the 180 isotherm at 400 °C. Therefore, the results from both thermal ramp-stop and thermal ramp-isothermal treatments demonstrate the utility of a TOP analysis on identifying the experimental conditions for maximum PE.

Conclusion

The use of thermal oxidation profiling to monitor SWNT properties over the decomposition range of raw and acid-refluxed samples has been performed. The onset of decomposition for raw SWNT-HO in the TGA data is shown to correspond directly to the decrease in SWNT mass retention (R) for the TOP. This result demonstrates that the underlying mechanism for thermal oxidation in raw soots is due to precombustion from the metal-catalyst impurities. Removal of the metal-catalyst impurities is, therefore, deemed to be paramount to a high SWNT purification efficiency. In comparison, acid-refluxed SWNT samples offer the ability to control the thermal treatment such that high purification efficiencies are easily achieved. It was demonstrated that the peak frequency of the G′-band in the Raman spectrum is a straightforward purification monitor to probe the acid doping during the reflux process. Purification efficiencies of 75% for select time and temperature conditions demonstrate the efficacy of a simple acid reflux and thermal oxidation for laser-produced SWNT purification. In addition, a general understanding of the SWNT thermal stability and decomposition kinetics for SWNT-containing materials has been obtained. The balance between time and temperature on thermal oxidation steps for acid-refluxed SWNTs was systematically identified to enhance purification monitoring. These unprecedented results on characterizing the purification process and quantifying the mass retention and purity can enable the reproducible production of high-quality SWNTs.

Acknowledgment. The authors wish to thank Jim Worman and Herb Ruf for helpful discussions during this work. Financial support for this project was made by BP Solar; the National Science Foundation, Grant No. ECS-0233776; NASA, Grant Nos. NAG3-2828, NCC3-956, and NNC05GA14G; and the Rochester Institute of Technology's First In Class Initiative. B.J.L. also acknowledges financial support from a NASA Graduate Student Research Fellowship.

CM052002U